AGU100 ADVANCING EARTH AND SPACE SCIENCE

Geochemistry, Geophysics, Geosystems

RESEARCH ARTICLE

10.1029/2018GC007552

Key Points:

- Heavy radiogenic isotopic data for 42 oceanic hot spots are evaluated as a function of hot spot location, including position over the LLSVPs
- Geochemically enriched (EM) hot spots are concentrated in the Southern Hemisphere, and HIMU hot spots are found near the tropical latitudes
- The two LLSVPs have remarkably similar EM compositions; EM hot spots are geographically associated with the LLSVPs, but HIMU hot spots are not

Supporting Information:

- Supporting Information S1
- Figure S1
- Figure S2
- Table S1
- Table S2

Correspondence to:
M. G. Jackson,
jackson@geol.ucsb.edu

Citation:
Jackson, M. G., Becker, T. W., & Konter, J. G. (2018). Geochemistry and distribution of recycled domains in the mantle inferred from Nd and Pb isotopes in oceanic hot spots: Implications for storage in the large low shear wave velocity provinces. *Geochemistry, Geophysics, Geosystems*, *19*, 3496–3519. https://doi.org/10.1029/2018GC007552

Received 13 MAR 2018
Accepted 20 AUG 2018
Accepted article online 31 AUG 2018
Published online 27 SEP 2018

Geochemistry and Distribution of Recycled Domains in the Mantle Inferred From Nd and Pb Isotopes in Oceanic Hot Spots: Implications for Storage in the Large Low Shear Wave Velocity Provinces

M. G. Jackson[1], T. W. Becker[2], and J. G. Konter[3]

[1]Department of Earth Science, University of California, Santa Barbara, CA, USA, [2]Institute for Geophysics and Department of Geological Sciences, The Jackson School of Geosciences, University of Texas at Austin, Austin, TX, USA, [3]Department of Geology and Geophysics, School of Ocean and Earth Science and Technology, University of Hawaiiat Manoa, Honolulu, HI, USA

Abstract Subduction of continental and oceanic crust is thought to give rise to geochemically distinct reservoirs in the mantle called EM (enriched mantle) and HIMU (high $\mu = {}^{238}U/{}^{204}Pb$), respectively. However, the locations of EM and HIMU domains in the Earth's interior are poorly constrained. We explore the geographic distribution of extreme EM (${}^{143}Nd/{}^{144}Nd \leq 0.512630$) and HIMU (${}^{206}Pb/{}^{204}Pb \geq 20$) geochemical signatures in ocean island basalts erupted at hot spots, highlighting three observations. First, hot spots geographically associated with the two large low shear wave velocity provinces (LLSVPs) have a similar range of EM compositions. If these hot spots are sourced by the LLSVPs via upwelling plumes, this observation is consistent with the hypothesis that the LLSVPs formed by similar processes and have similar geodynamic histories. Second, the EM and HIMU domains exhibit different latitudinal zonation: oceanic hot spots with the most extreme EM compositions (${}^{143}Nd/{}^{144}Nd < 0.5125$) are concentrated in the Southern Hemisphere (14°S to 52°S latitude), while oceanic hot spots hosting HIMU compositions are found primarily near the tropical latitudes (38°N to 29°S). Third, all 13 oceanic hot spots with EM compositions (${}^{143}Nd/{}^{144}Nd \leq 0.512630$) are geographically associated with the LLSVPs; oceanic hot spots located far from the LLSVPs exhibit only non-EM (${}^{143}Nd/{}^{144}Nd > 0.512630$) compositions. In contrast, the HIMU domains do not show a clear geographic association with the LLSVPs. Therefore, EM and HIMU domains in the Earth's mantle exhibit different spatial distributions. This may reflect differences in subduction inputs of these two components, or differences in how they segregate or accumulate in the deep Earth.

1. Introduction

The Earth's mantle is compositionally heterogeneous and exhibits geochemical heterogeneity at a variety of length scales (e.g., Hart, 1988; Hofmann, 1997; Stracke, 2012; Stracke et al., 2005; White, 2015; Zindler & Hart, 1986). Geochemically enriched (i.e., EM, or enriched mantle) and HIMU (high $\mu = {}^{238}U/{}^{204}Pb$) mantle domains, which are thought to result from convective recycling of continentally derived material and oceanic lithosphere, respectively, are globally distributed in the Earth's mantle (e.g., Hart, 1984; Homrighausen et al., 2018) at a variety of length scales: radiogenic isotopic heterogeneity is observed at the submeter scale in peridotites (e.g., Harvey et al., 2006; Liu et al., 2008; Warren, 2016; Warren & Shirey, 2012), and at the longest length scales, including hemispheric (i.e., spherical harmonic degree-2) patterns of geochemical heterogeneity sampled by hot spots. For example, Hart (1984) observed that hot spots located within a globe-encircling belt in the Southern Hemisphere tend to exhibit signatures of geochemical enrichment. Referred to as the DUPAL (Dupré & Allègre, 1983) anomaly—the most geographically extensive terrestrial isotopic domain observed—Hart (1984) showed that hot spots exhibiting extreme geochemical enrichment cluster in the South Atlantic, the Indian, and the South Pacific Ocean basins. Hart (1988) included both EM and HIMU compositions in defining the geographic distribution of DUPAL and showed that the geographic distribution of the DUPAL anomaly is generally shifted to the Southern Hemisphere. However, the origin of the DUPAL geochemical domain, and how it is preferentially sampled by hot spots in the Southern Hemisphere, remains poorly understood.

An important advance in the understanding of the DUPAL anomaly emerged from the work of Castillo (1988), who showed that geochemically enriched hot spots located within the DUPAL anomaly tend to overlie two large, deep, near-antipodal mantle structures characterized by anomalously low seismic velocity anomalies, now called large low shear wave velocity provinces (LLSVPs). One model for the geographic relationship between seismic anomalies at depth and geochemical enrichment in hot spots situated above the LLSVPs is that the geochemically enriched domains sampled by hot spots originate in the LLSVPs. In this model, upwelling mantle plumes—which are inferred to emerge from the deep mantle (e.g., Boschi et al., 2007; French & Romanowicz, 2015; Montelli et al., 2006; Weis et al., 2011)—entrain geochemically enriched material from the LLSVPs and transport this material to the shallow region of mantle melting beneath hot spot volcanoes. This model helps to explain why some plume-sourced hot spots that overlie the LLSVPs erupt lavas with geochemically enriched (EM) signatures, while hot spots that do not overlie the LLSVPs fail to exhibit these signatures.

It has been three decades since Castillo's (1988) work relating geophysical observations of the seismic structure of the mantle with the geochemistry of mantle-derived lavas at the surface. However, the geochemical structure of the Earth's interior remains uncertain. This is because the geochemical compositions of plume-fed hot spot lavas do not provide constraints on the depth of mantle reservoirs sampled by the lavas. Similarly, seismic models provide constraints on the structure of the Earth's interior but they cannot resolve isotopic heterogeneities.

The two LLSVPs cover just ~25% of the core-mantle boundary, yet most hot spots overlie the LLSVPs, an observation that suggests a possible connection between hot spots and LLSVPs (e.g., Hager et al., 1985; Ritsema et al., 2011; Thorne et al., 2004; Torsvik et al., 2006; Williams et al., 1998). If hot spots are fed by mantle plumes that upwell from the core-mantle boundary and entrain material from the LLSVPs (e.g., Hernlund & McNamara, 2015), then the radiogenic isotopic geochemistry of oceanic hot spots provides an opportunity to investigate the composition of the LLSVPs. Establishing geographic relationships between the geochemistry of hot spots and their position with respect to the LLSVPs is important to evaluate models arguing that plume fed hot spots sample material conveyed from the LLSVPs, and would permit inferences to be made about the composition of seismically observed structures in the deep Earth and provide information about the thermochemical evolution of the mantle (e.g., Castillo, 1988; Konter & Becker, 2012). Furthermore, observations about the global distribution of geochemical domains sampled by oceanic hot spots are of fundamental importance in chemical geodynamics and provide a primary constraint for geodynamic models that attempt to describe the evolution of the Earth's interior.

In this study, we take advantage of recent, higher-resolution seismic models and greatly expanded geochemical data sets to test the hypothesis that geochemical enrichment observed in oceanic hot spot lavas relates to a hot spot's geographic relationship to the LLSVPs. Here we build on the established relationship between extreme EM and HIMU compositions and seismically detectable plumes (Jackson et al., 2018). We compare Jackson et al.'s (2018) compiled geochemical database of the highest ^{206}Pb/^{204}Pb and lowest (i.e., most geochemically enriched) ^{143}Nd/^{144}Nd lavas from 42 oceanic hot spots with new seismic shear wave velocity models of the base of the mantle (see Tables 1 and S1 and S2 in the supporting information).

Castillo (1988) evaluated whether signatures of geochemical enrichment—including ^{87}Sr/^{86}Sr, Δ^{207}Pb/^{204}Pb, and Δ^{208}Pb/^{204}Pb (where Δ^{207}Pb/^{204}Pb and Δ^{208}Pb/^{204}Pb are derived Pb isotopic parameters that correlate positively with ^{87}Sr/^{86}Sr among ocean island basalts (OIBs) globally; Hart, 1984)—are geographically associated with the LLSVPs. However, he left evaluating examination of extreme high ^{206}Pb/^{204}Pb and low ^{143}Nd/^{144}Nd signatures to future work. In light of $>$30 years of additional radiogenic isotopic data gathered on oceanic hot spot lavas, we examine the geochemistry of oceanic hot spot lavas to evaluate the distribution of maximum ^{206}Pb/^{204}Pb (a proxy for a contribution from the HIMU domain in the mantle), and the distribution of minimum ^{143}Nd/^{144}Nd (a proxy for a contribution from the EM domain), to evaluate whether EM and HIMU domains have similar, or different, geographic distributions. We evaluate whether the most extreme EM and HIMU oceanic hot spots exhibit geographic patterns as a function of latitude and longitude, and whether extreme EM and HIMU compositions are geographically associated with the LLSVPs. Furthermore, we examine whether the two LLSVPs—the one under Africa, the Atlantic, and Indian Oceans (here referred to as the Atlantic LLSVP) or the one under the Pacific—have similar or different extreme EM or HIMU compositions.

Table 1
The Locations of the 42 Oceanic Hot Spots Examined in This Study and Their Distances From the LLSVPs

Hot spot	Hot spot #[a]	Hot spot latitude[b]	Hot spot longitude[b]	Distance from LLSVP (km) SMEAN2, 0.75RMS[c]	Which LLSVP?[d]	Distance from LLSVP (km; Lekic et al., 2012)
Arago-Rurutu	1	−23.5	−150.7	−1,663	Pacific	−1,824
Amsterdam-St. Paul	2	−37.0	78.0	−631	Atlantic	−685
Ascension	3	−8.0	−14.0	−606	Atlantic	−1,015
Azores	4	38.0	−28.0	483	Near Atlantic	143
Baja-Guadalupe	5	27.0	−113.0	2,885	Far from LLSVP	2,785
Balleny	6	−67.4	164.7	2,765	Far from LLSVP	3,515
Bouvet	7	−54.4	3.4	740	Near Atlantic	607
Bowie-Pratt Welker	8	49.5	−130.0	3,651	Far from LLSVP	3,892
Cameroon	9	−1.0	6.0	−610	Atlantic	−667
Canary	10	28.0	−17.0	−852	Atlantic	−1,118
Cape Verde	11	15.0	−24.0	−217	Atlantic	−492
Caroline	12	5.3	163.0	−1,239	Pacific	−1,269
Cobb-Axial-Juan de Fuca	13	43.6	−128.7	3,599	Far from LLSVP	3,435
Comores	14	−12.0	44.0	1,024	Near Atlantic	551
Crozet	15	−46.0	50.0	−113	Atlantic	−759
Discovery	16	−44.5	−6.5	114	Near Atlantic	−49
Easter	17	−27.0	−109.0	−1,042	Pacific	50
Fernando de Noronha	18	−4.0	−32.0	1,277	Near Atlantic	881
Galapagos	19	−0.4	−92.0	745	Near Pacific	366
Great Meteor-New England	20	31.0	−28.5	37	Near Atlantic	−83
Hawaii	21	18.9	−155.3	331	Near Pacific	49
Heard	22	−49.0	63.0	−462	Atlantic	−695
Iceland	23	64.6	−17.6	−157	Atlantic	39
Jan Mayen	24	71.7	−8.0	357	Near Atlantic	608
Juan Fernandez	25	−34.0	−79.0	1,407	Near Pacific	1,303
Louisville	26	−53.5	−141.2	1,016	Near Pacific	346
Macdonald	27	−29.0	−140.4	−1,415	Pacific	−828
Madeira	28	32.7	−17.5	−516	Atlantic	−769
Manus Basin-Indonesia	29	−3.8	149.7	−1,352	Pacific	−976
Marion-Prince Edward	30	−46.8	37.8	209	Near Atlantic	−28
Marquesas	31	−11.5	−137.5	−703	Pacific	−611
Martin Vas-Trindade	32	−20.0	−29.0	1,105	Near Atlantic	−78
Meteor-Shona	33	−52.0	1.0	494	Near Atlantic	308
Pitcairn	34	−25.3	−129.3	−1,930	Pacific	−50
Rarotonga	35	−21.5	−159.7	−832	Pacific	−1,508
Reunion	36	−21.0	55.5	265	Near Atlantic	364
Samoa	37	−14.3	−169.0	−771	Pacific	−1,240
San Felix	38	−26.0	−80.0	1,028	Near Pacific	708
Societies	39	−18.3	−148.0	−2042	Pacific	−1,967
Socorro-Revillagigedo	40	19.0	−111.0	1,982	Near Pacific	1,877
St Helena	41	−17.0	−10.0	−741	Atlantic	−1,428
Tristan-Gough	42	−40.3	−10.0	85	Near Atlantic	−72

[a]The hot spot number is used to identify hot spots in Figure 1. [b]All hot spots and locations are after King and Adam (2014), except for the Manus Basin hot spot, which is added to the hot spot catalogue here. [c]Distances are provided between each hot spot (using the latitude and longitude provided in the table) and the margin of the nearest LLSVP, where the margins of the LLSVPs are defined for the SMEAN2 seismic model (0.75 RMS velocity contour), as discussed in the text. Negative distances are recorded for hot spots that lie within the margins of the LLSVPs, and positive distances are recorded for hot spots that lie outside of the margins of the LLSVPs. [d]The LLSVP designation of a hot spot is determined using the SMEAN2 seismic model: Hot spots that have negative distances from the margins of the Atlantic or Pacific LLSVPs (i.e., lie within the margins of the LLSVPs) are referred to as *Atlantic* or *Pacific* in the table; hot spots that have positive distances from the margins of the Atlantic or Pacific LLSVPs (i.e., lie outside the margins of the LLSVPs) are referred to as *near Atlantic* or *near Pacific* LLSVPs in the table; the four hot spots located farthest outside of the margins of the LLSVPs are called *far from LLSVP* hot spots. These criteria can also be used to establish the relationship of a hot spot with the large low shear wave velocity provinces (LLSVPs; i.e., Atlantic, Pacific, near-Atlantic, near Pacific, or far from LLSVP) using distances provided in the table for the Lekic et al. (2012) model (see supporting information Tables S1 and S2).

2. Methods

2.1. Hot Spot Catalogue and Selection of Lavas With Lowest $^{143}Nd/^{144}Nd$ and Highest $^{206}Pb/^{204}Pb$ From Each Oceanic Hotspot

King and Adam (2014) provide one of the most comprehensive, recent compilations of global hot spots, which includes 54 hot spots total. We rely on the King and Adam (2014) compilation and add one additional hot spot—the Manus Basin hot spot—which erupts moderately high $^{3}He/^{4}He$ lavas (Macpherson et al., 1998) and is found to be associated with a plume conduit (the "Indonesia" plume in French & Romanowicz, 2015). Of these 55 hot spots, only 9 hot spots are continental: Australia East, Darfur, Eifel, Hoggar, Raton-Jemez, Tibesti, Yellowstone, Afar, and East Africa. Those continental hot spots are not considered here, owing to (1) the potential for continental crust overprinting of the mantle-derived radiogenic isotopic signatures in these lavas and (2) the potential for continental lithosphere to inherit and preserve EM and HIMU signatures (e.g., from ancient plumes) that may be incorporated into more recent continental volcanism. Excluding continental hot spots does not significantly impact the hot spot database or the conclusions of this study, as only ~16% of the hot spots in the database are continental. After excluding the nine continental hot spots, we are left with 46 oceanic hot spots, 4 of which lack complete geochemical data sets: Vema, Bermuda, Tasmantid-Tasman Central, and Lord Howe-Tasman East. Thus, 42 geochemically characterized oceanic hot spots with available Sr, Nd, and Pb isotopic data remain for analysis in this study. The geochemical database for 42 oceanic hot spots explored is provided in Jackson et al. (2018; see Table 1 for list of hot spots), and the locations of the hot spots are shown in Figure 1 (see supporting information Tables S1 and S2).

Jackson et al. (2018) identified a lava with the lowest $^{143}Nd/^{144}Nd$ and a lava with the highest $^{206}Pb/^{204}Pb$ from each of 42 oceanic hot spots (see supporting information Tables S1 and S2). However, some of the oceanic hot spots examined here sample a variety of geochemical compositions (e.g., Comores and Cape Verde), and at these hot spots, no single lava captures both the lowest $^{143}Nd/^{144}Nd$ *and* the highest $^{206}Pb/^{204}Pb$ components at each hot spot. As discussed in Jackson et al. (2018), in order to better capture the geochemical extremes at each hot spot, a lava with the highest $^{206}Pb/^{204}Pb$ *and* a lava with the lowest $^{143}Nd/^{144}Nd$ are selected from each of these hot spots. However, for a number of hot spots, a single lava captures the most extreme low $^{143}Nd/^{144}Nd$ and high $^{206}Pb/^{204}Pb$ signatures (e.g., Easter and San Felix, etc.), so it was not necessary to select two lavas at these hot spots.

HIMU hot spots are defined to have $^{206}Pb/^{204}Pb \geq 20$, a threshold that is higher than DMM (depleted MORB [mid-ocean ridge basalt] mantle) and the upper range of possible values for the FOZO (focus zone; Hart et al., 1992) and C (common; Hanan & Graham, 1996) components. While it may be preferable to use the bulk silicate Earth $^{206}Pb/^{204}Pb$ composition as the threshold for the HIMU domain, this composition is not well constrained. Thus, we use the upper limit (high $^{206}Pb/^{204}Pb$) of the FOZO-C component to define the low $^{206}Pb/^{204}Pb$ threshold value for HIMU. Stracke et al. (2005) estimated the $^{206}Pb/^{204}Pb$ composition of the common (FOZO-C) component to be as high as 20.5. However, in a more recent study, Konter et al. (2008) quantified the radiogenic isotopic composition of the common component in OIBs by determining the best fit volume that encompasses the intersection of global OIB arrays in Sr-Nd-Pb multi-isotopic space, and they determined that the "center" (i.e., FOZO-C) component has a $^{206}Pb/^{204}Pb$ composition of 19.238 ± 0.738 (or 18.500 to 19.976). Moreover, we are not aware of any OIB with $^{206}Pb/^{204}Pb \geq 20$ that also exhibit elevated $^{3}He/^{4}He$, a characteristic ascribed to the FOZO-C common component. While any strict threshold for the HIMU composition is arbitrary, an upper limit for the $^{206}Pb/^{204}Pb$ of the FOZO-C component is 19.976. Therefore, we use this value as a conservative lower limit for the HIMU composition, and OIBs with $^{206}Pb/^{204}Pb \geq 20$ are designated as HIMU in composition.

Hot spots that host at least one lava sampling extreme high $^{206}Pb/^{204}Pb$ ratios (≥20) are designated as HIMU hot spots, and only 13 or the 42 oceanic hot spots satisfy this condition: Arago-Rurutu, Azores, Baja-Guadalupe, Cameroon, Canary, Cape Verde, Comores, Easter, Galapagos, Great Meteor-New England, Macdonald, Marquesas, and St. Helena. If we use a higher $^{206}Pb/^{204}Pb$ threshold for the HIMU component, where HIMU hot spots have $^{206}Pb/^{204}Pb \geq 20.4$, then only eight hot spots are classified as HIMU hot spots: Macdonald, St. Helena, Cameroon, Azores, Arago-Rurutu, Easter, Greater Meteor-New England, and St. Helena.

There exists a geochemical continuum between the EM1 and EM2 mantle endmember compositions in Sr, Nd, and Pb isotopic space (Stracke et al., 2005), and we do not attempt to distinguish between the EM1 and EM2 endmember compositions here. Instead we seek to identify the lavas with the lowest (most geochemically enriched) $^{143}Nd/^{144}Nd$ from each hot spot, and this selection is made irrespective of its EM1 or EM2 designation (Jackson et al., 2018). The threshold Nd-isotopic value for EM hot spots is based on the chondritic $^{143}Nd/^{144}Nd$ ratio (0.512630; Bouvier et al., 2008), where lavas with $^{143}Nd/^{144}Nd > 0.512630$ are

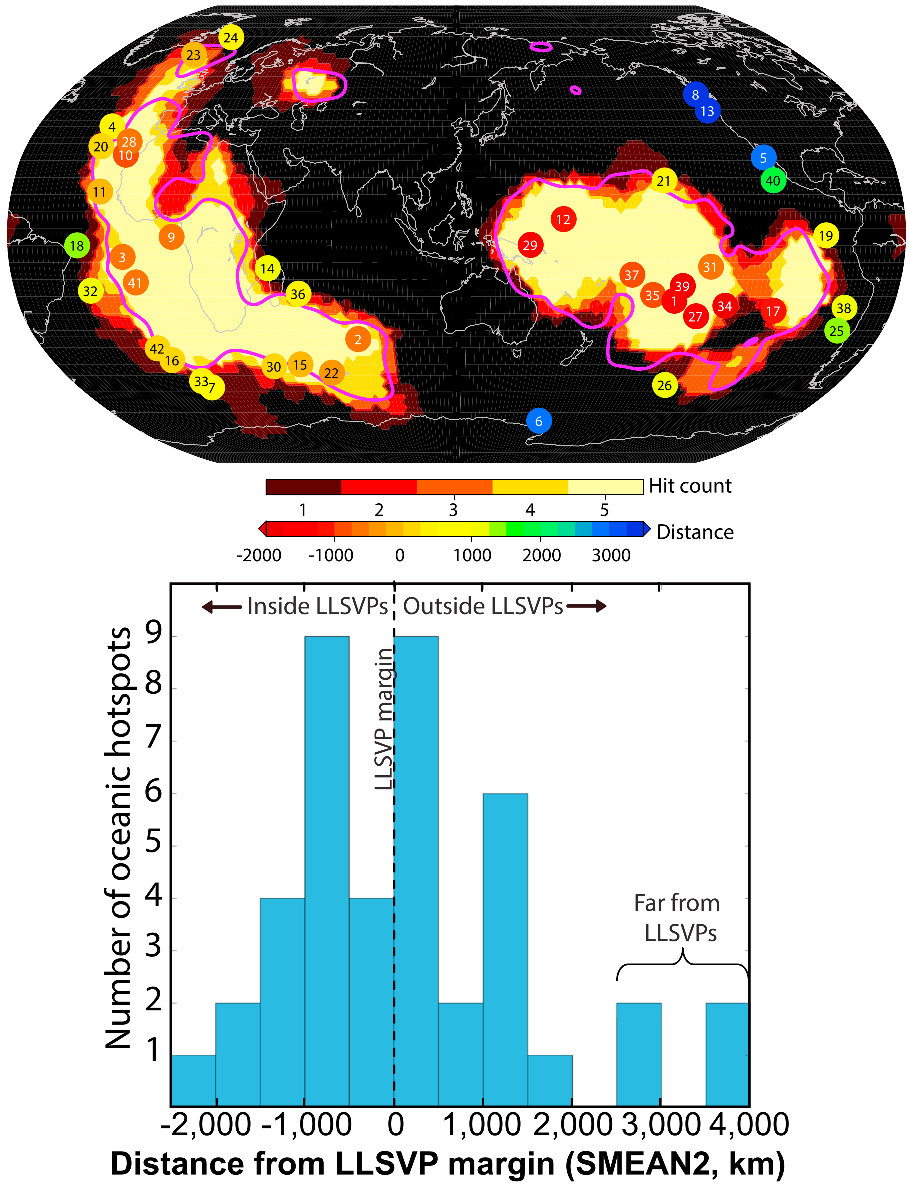

Figure 1. (top panel) The 42 oceanic hot spots considered in this study are shown as circles on the map, and the number inside the circle identifies the hot spot (see "hot spot #" in Table 1). The color of the circle indicates the minimum distance of a hot spot from the nearest large low shear wave velocity province (LLSVP) margin using the SMEAN2 composite tomography model. The 75% of RMS velocity contour for SMEAN2 at 2,875-km depth is shown as a pink line and defines the LLSVP margin for this study. The LLSVP "stack" from Lekic et al. (2012) is shown for reference, where higher "hit counts" for LLSVP detection (for the five seismic models used in the stack) are shown with brighter colors. (bottom panel) The histogram shows the distribution of hot spot distances from the LLSVP margins defined using SMEAN2: Negative distances indicate that hot spots are located inside of the margins of the LLSVPs (and such hot spots are referred to as "LLSVP hot spots"), while positive distances indicate that hot spots are located outside of, but near, the margins of the LLSVPs (and such hot spots are referred to as "near LLSVP hot spots"). However, the four hot spots located farthest from the LLSVP margins—Bowie-Pratt Welker, cobb-axial-Juan de Fuca, Balleny, and Baja-Guadalupe—do not cluster together with the rest of the hot spots in the histogram and are referred to as "far from LLSVP" hot spots.

considered geochemically depleted (and are referred to as non-EM). Hot spots with at least one lava sampling low (geochemically enriched) $^{143}Nd/^{144}Nd$ ratios ($\leq$ 0.512630) are designated as EM hot spots, and 13 of the 42 oceanic hot spots satisfy this condition: Amsterdam-St. Paul, Cape Verde, Comores, Discovery, Hawaii, Heard, Meteor-Shona, Pitcairn, Rarotonga, Samoa, San Felix, Societies, and Tristan-Gough.

We note that future work could examine different threshold $^{143}Nd/^{144}Nd$ and $^{206}Pb/^{204}Pb$ values for the EM and HIMU domains, respectively. Similarly, $^{87}Sr/^{86}Sr$ (Castillo, 1988), or a trace element ratio, could be used to classify OIB as geochemically "enriched" or "depleted", but the former is more susceptible to seawater alteration than $^{143}Nd/^{144}Nd$ and the latter is sensitive to melting and crystal fractionation processes. Additionally, we limit our study to isotopic compositions measured in basalts: if an EM or HIMU component has been hypothesized to exist in the mantle source of a particular hot spot but has not actually been observed in basalts from the hot spot locality (because, e.g., the hypothetical component has been diluted by less geochemically extreme melts), then the hot spot is not classified as geochemically EM or HIMU. For example, an enriched component has been suggested to exist in the mantle source of the Iceland hot spot (e.g., Hanan & Schilling, 1997; Kokfelt et al., 2006), but lavas that satisfy the geochemical criteria for EM lavas in this study (i.e., $^{143}Nd/^{144}Nd$ ratios $\leq$0.512630) have not been observed in Iceland, and we do not classify Iceland as an EM hot spot.

Figure 2 shows the highest $^{206}Pb/^{204}Pb$ (most extreme HIMU) and the lowest $^{143}Nd/^{144}Nd$ (most extreme EM signature) lavas from each of 42 oceanic hot spots in map view. The highest $^{206}Pb/^{204}Pb$ and lowest $^{143}Nd/^{144}Nd$ lavas for each hot spot are shown in Figure 3, in order of decreasing $^{206}Pb/^{204}Pb$ and increasing $^{143}Nd/^{144}Nd$, respectively, and the data are color coded depending on whether a hot spot is geographically associated with the Atlantic LLSVP (red symbols), the Pacific LLSVP (blue symbols), or neither LLSVP (black symbols) if the hot spot is located far from of the LLSVPs (see section 2.2). All isotopic compositions plotted are provided in supporting information Tables S1 and S2.

2.2. Hot Spot Association With Seismically Constrained Atlantic or Pacific LLSVPs

In order to compare oceanic hot spot compositions with seismically defined structures, presumably connected by plumes, it is preferable to consider more than one tomographic model, given the range of inversion choices, uneven data coverage, and different methodological approaches. Instead, such a comparison can be more robustly accomplished using a definition of the LLSVPs from mean, composite models, or by considering a "vote map" across several models. We explore both approaches.

We seek to evaluate whether each of the 42 oceanic hot spots is geographically associated with (i.e., within the margins or outside of but near the margins) the Atlantic or Pacific LLSVPs. It is then necessary to evaluate the boundaries of the LLSVPs, and for this purpose we, first, use the SMEAN2 seismic shear wave tomography model as described in Jackson et al. (2017). SMEAN2 was constructed using the same methods as the composite SMEAN model (Becker & Boschi, 2002) with the goal of identifying common mantle structure across several different seismic shear wave velocity models (Qin et al., 2009). As discussed in Jackson et al. (2017), SMEAN2 combines S40RTS (Ritsema et al., 2011), GyPSum-S (Simmons et al., 2010), and SAVANI (Auer et al., 2014). The SMEAN2 model can be found at http://www-udc.ig.utexas.edu/external/becker/tdata.html.

We choose the 75% of root mean square (RMS) velocity contour at the deepest model depth, 2,875 km, in SMEAN2 to define margins of the LLSVPs, which corresponds to a -0.8% δV_S velocity anomaly at this depth (see Figure 1). Using this definition, 25% of the surface area of the core-mantle boundary is covered by LLSVPs. When projected radially to the surface, 20% of the area encompassed by the margins of the LLSVPs is under the continents and 80% is under the oceans (using the land-sea boundary in Generic Mapping Tools). Only 29% of the ocean is underlain by LLSVPs when they are radially projected to the surface, while just 18% of the continents are underlain by LLSVPs.

Other methods for defining the outline of the LLSVPs exist. For example, Torsvik et al. (2006) use the -1% δV_S velocity anomaly of SMEAN at the core-mantle boundary to define the boundaries of the LLSVPs. Any such contour value is somewhat arbitrary, and its interpretation (e.g., in terms of temperature or composition) is influenced by the resolution and damping choices of tomographic imaging.

For comparison, we therefore also consider the LLSVP "hitcount" stack from Lekic et al. (2012; Figure 1). Lekic et al. (2012) consider five tomography models to evaluate the presence of an LLSVP, and at each location there is a count as to how many models indicate the presence of an LLSVP. The 75% of RMS velocity contour for SMEAN2 generally shows good agreement with the 3 hit count in the Lekic et al. (2012) stack (where the choice of "3" in the Lekic stack represents a "three-fifths majority vote"; Figure 1).

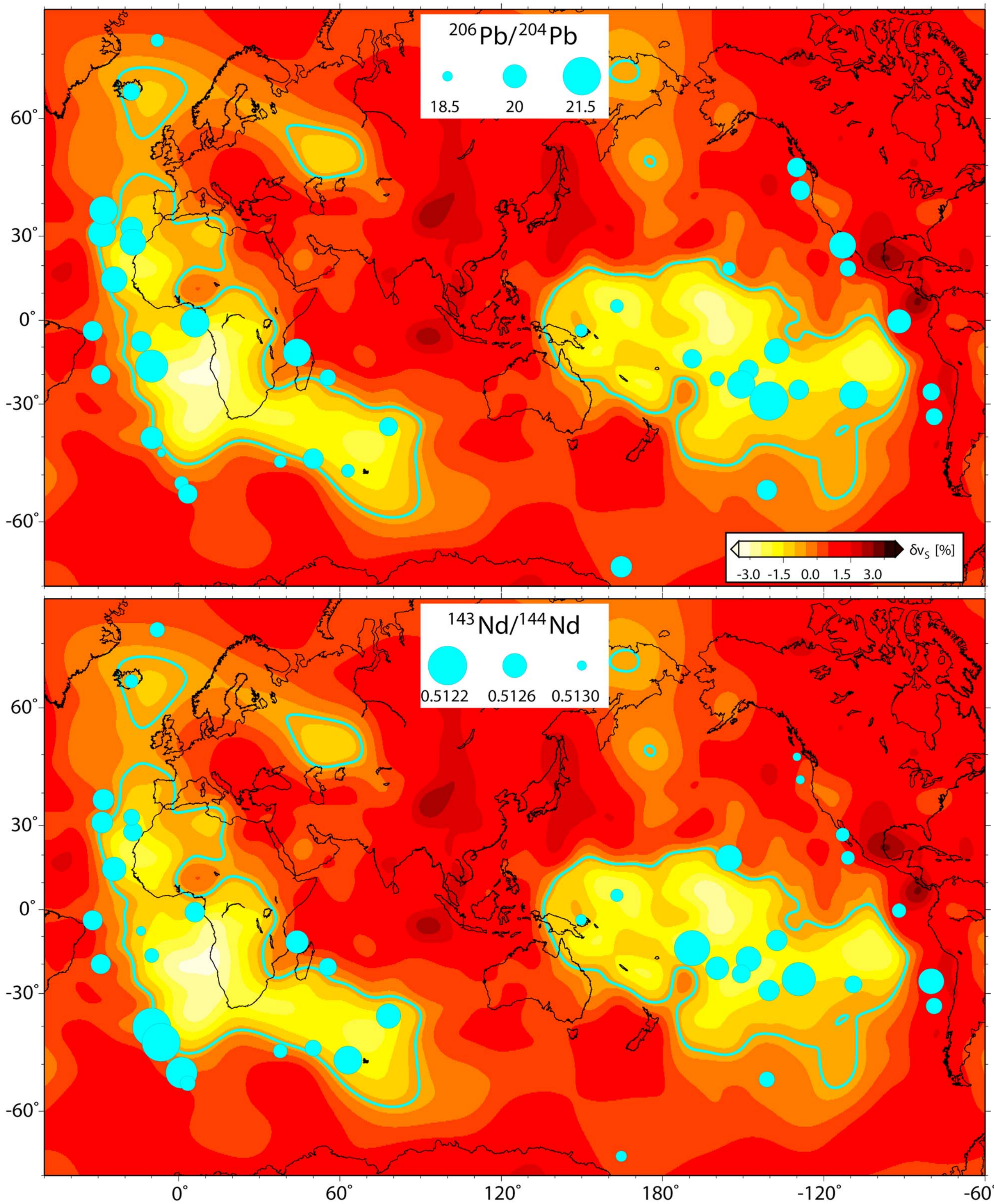

Figure 2. The minimum ^{143}Nd/^{144}Nd (top panel) and maximum ^{206}Pb/^{204}Pb (bottom panel) isotopic compositions at each of the 42 geochemically characterized oceanic hot spots are shown on a map. The hot spots with the lowest ^{143}Nd/^{144}Nd (i.e., the most geochemically enriched) are shown with the largest symbols; the lavas with the highest ^{206}Pb/^{204}Pb (i.e., the most extreme HIMU) are shown with the largest symbols. Radiogenic isotopic values shown are presented in supporting information Tables S1 and S2. The background shows velocity contours for the SMEAN2 composite tomography model at 2,875-km depth, and the 75% of RMS velocity contour, which is $\delta V_s = -0.8\%$ (i.e., the working definition of the large low shear wave velocity province margin in this study), is shown as a light blue line HIMU = high μ = ^{238}U/^{204}Pb.

10.1029/2018GC007552

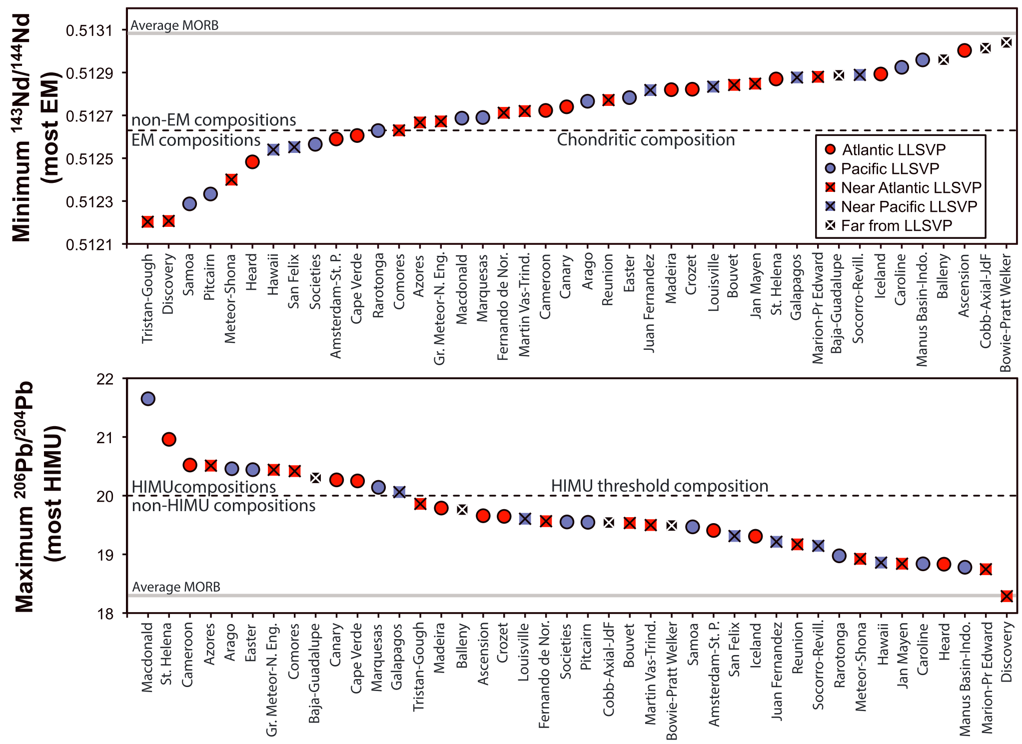

Figure 3. The minimum $^{143}Nd/^{144}Nd$ (upper panel) and maximum $^{206}Pb/^{204}Pb$ (lower panel) compositions for each of 42 oceanic hot spots (supporting information Tables S1 and S2). The 75% of RMS velocity contour at 2,875-km depth in the SMEAN2 seismic model is used to define the LLSVP margins for hot spot classification in this figure: Hot spots geographically associated with the two LLSVPs—Atlantic (red symbols) and Pacific (blue symbols)—are shown with different colors, and the four hot spots located farthest from the LLSVPs (and not clearly associated with either LLSVP) are shown as black squares; hot spots located inside the LLSVPs (circles) and outside but near (squares) the two LLSVPs are shown with different symbols. The global average MORB composition (all MORB located far from hot spots, and excluding back arc basin lavas; Gale et al., 2013) is shown with a solid gray line in both panels. The threshold values for EM ($^{143}Nd/^{144}Nd$ = 0.512630) and HIMU hot spots ($^{206}Pb/^{204}Pb$ = 20) are shown with a thin black dashed line in both panels. See supporting information Tables S1 and S2 for hot spots compositions. EM = enriched mantle; HIMU = high $\mu = {}^{238}U/^{204}Pb$; LLSVP = large low shear wave velocity province.

Figure 1 shows the locations of the 42 oceanic hot spots together with a histogram of hot spot distances from the SMEAN2-defined LLSVP boundary (Table 1): negative distances indicate that hot spots are located inside the LLSVPs (positive distances are outside). While 38 of the 42 oceanic hot spots cluster near the margins of the LLSVPs, 4 of the 42 hot spots—Balleny (located 2,765 km from the LLSVP margin), Baja-Guadalupe (2,885 km), Cobb-Axial-Juan de Fuca (3,599 km), and Bowie-Pratt Welker (3,651 km)—plot away from the cluster of LLSVP and near-LLSVP hot spots on the histogram. These four outlying hot spots are referred to hereafter as being located "far from the LLSVPs" (see Table 1).

The 38 oceanic hot spots that cluster near the margins of the LLSVPs (see histogram in Figure 1) defined for SMEAN2 are described as being geographically associated with the LLSVPs: 20 of these hot spots are located within the margins of the LLSVPs (and are called "LLSVP hot spots" hereafter), and 18 are located outside of the LLSVPs but near the LLSVP margins (and are referred to as *near-LLSVP hot spots*). In the SMEAN2 model, 22 of the hot spots are geographically associated with the Atlantic LLSVP margin and 16 are associated with the Pacific LLSVP.

We also compute hot spot distances from LLSVP margins from Lekic et al. (2012), for which we define the distance between a hot spot and the margins of the LLSVPs as the minimum distance to a contour traced by at least a hit count of three. Hot spot distances from the margins of the LLSVPs calculated using the Lekic et al. (2012) stack are quantitatively different from the SMEAN2 approach (see supporting information Tables S1 and S2). Nonetheless, a hot spot's geographic association with a particular LLSVP, Atlantic or Pacific, is maintained irrespective of the approach, but we note that five near-LLSVP hot spots in the SMEAN2 model are located within the LLSVP margins of the Lekic et al. (2012) stack (e.g., Discovery, Great Meteor-New England, Marion-Prince Edward, Martin Vas-Trindade, and Tristan-Gough), and two LLSVP hot spots in the SMEAN2 model are near-LLSVP hot spots in the Lekic et al. (2012) model (e.g., Easter and Iceland). The classification of Baja-Guadalupe, Balleny, Bowie-Pratt-Welker, and Cobb-Axial-Juan de Fuca as "far from the LLSVPs" is consistent for both LLSVP definitions.

If hot spots are sourced by plumes that originate in the deep mantle, it can be argued that the hot spots overlying the LLSVPs are sourced by these deep mantle structures. However, it is uncertain whether hot spots that are located outside of, but near, the LLSVP margins are linked with the LLSVPs. Owing to uncertainties in the precise locations of the LLSVP boundaries (see Figure 1 and supporting information Tables S1 and S2), some hot spots located outside of the LLSVP margins defined in a particular seismic model may be fed by plumes that actually originate within the LLSVPs. Moreover, the geochemical reservoirs of relevance may be associated with compositional rather than thermally or seismically defined deep mantle anomalies, and those are expected to be only a fraction of the LLSVP (e.g., Hernlund & McNamara, 2015).

There are, of course, other uncertainties in relating surface hot spot locations with deep mantle plume sources, such as plume conduit deflection in the mantle and relative motion of the near-surface plume with respect to the current hot spot location (Boschi et al., 2007; Konrad et al., 2018; Steinberger & Antretter, 2006). Konter and Becker (2012) used advected plumes to compare Sr, Nd, and Pb isotopic compositions in hot spot lavas with seismic velocity anomalies at depth. However, due to the uncertainties associated with plume advection, we do not take this approach, and we do not explore any detailed relationships such as whether hot spots are sourced over the interior or the margins of the LLSVPs here (see, e.g., Austermann et al., 2014; Burke et al., 2008; Thorne et al., 2004). Instead, we use the overall hot spot and LLSVP locations to define whether or not an oceanic hot spot is generally associated with the LLSVPs.

2.3. Oceanic Hotspot Association With Plumes

While 31 of the 42 (or 74%) of the oceanic hot spots considered here (including LLSVP, near-LLSVP, and far from LLSVP hot spots) are associated with a plume in at least one of the three plume catalogues considered by Jackson et al. (2018; see supporting information Tables S1 and S2), plumes are not detected under 11 of the oceanic hot spots in any of the catalogues. The nondetection of a plume could mean that no plume exists beneath a hot spot. However, it could also mean that the plume conduit is too narrow (e.g., thermal plumes are thought to be narrower than thermochemical plumes; Kumagai et al., 2008) to be identified with existing seismic methods or that seismic coverage in the region is insufficient to resolve a plume. While existing plume catalogues do not allow us to demonstrate that every hot spot is fed by a plume that sources the deep mantle, the plume catalogues do provide support for the notion that most of the hot spots examined in this study are sourced by the deep mantle.

Below, we evaluate whether (1) the near-LLSVP hot spots have geochemical signatures that are similar to, or distinct from, the LLSVP hot spots and (2) whether the oceanic hot spots that are located far from the LLSVPs have different geochemical signatures than the LLSVP and near-LLSVP hot spots. To evaluate these questions, the Atlantic and Pacific LLSVP hot spots (red and blue circles, respectively) are shown with different symbols than the near-LLSVP hot spots (red and blue squares, respectively) in the figures (see, e.g., Figures 3–7). The hot spots located far from the LLSVPs are shown as black squares.

3. Observations

The lowest $^{143}Nd/^{144}Nd$ (Figure 4) and the highest $^{206}Pb/^{204}Pb$ (Figure 5) lava from each of the 42 oceanic hot spots are shown in multi-isotope space, including $^{143}Nd/^{144}Nd$ versus $^{206}Pb/^{204}Pb$, $^{87}Sr/^{86}Sr$ versus $^{206}Pb/^{204}Pb$, $^{207}Pb/^{204}Pb$ versus $^{206}Pb/^{204}Pb$, $^{208}Pb/^{204}Pb$ versus $^{206}Pb/^{204}Pb$, $^{143}Nd/^{144}Nd$ versus $^{87}Sr/^{86}Sr$, and $\Delta^{207}Pb/^{204}Pb$ versus $\Delta^{208}Pb/^{204}Pb$. The geochemically extreme lavas from the 42 hot spots capture the full spectrum of EM (Figure 4) and HIMU (Figure 5) compositions sampled by global oceanic lavas. A key observation is that hot spots geographically associated with the two LLSVPs exhibit a similar range of overlapping EM and HIMU compositions. Below we examine how the most extreme low $^{143}Nd/^{144}Nd$ and high $^{206}Pb/^{204}Pb$ compositions at each of the 42 oceanic hot spots considered here vary as a function of longitude, latitude, and distance from the margins of the LLSVPs. For our analysis, we rely on the SMEAN2 approach and also compare with results based on Lekic et al.'s (2012) analysis for completeness.

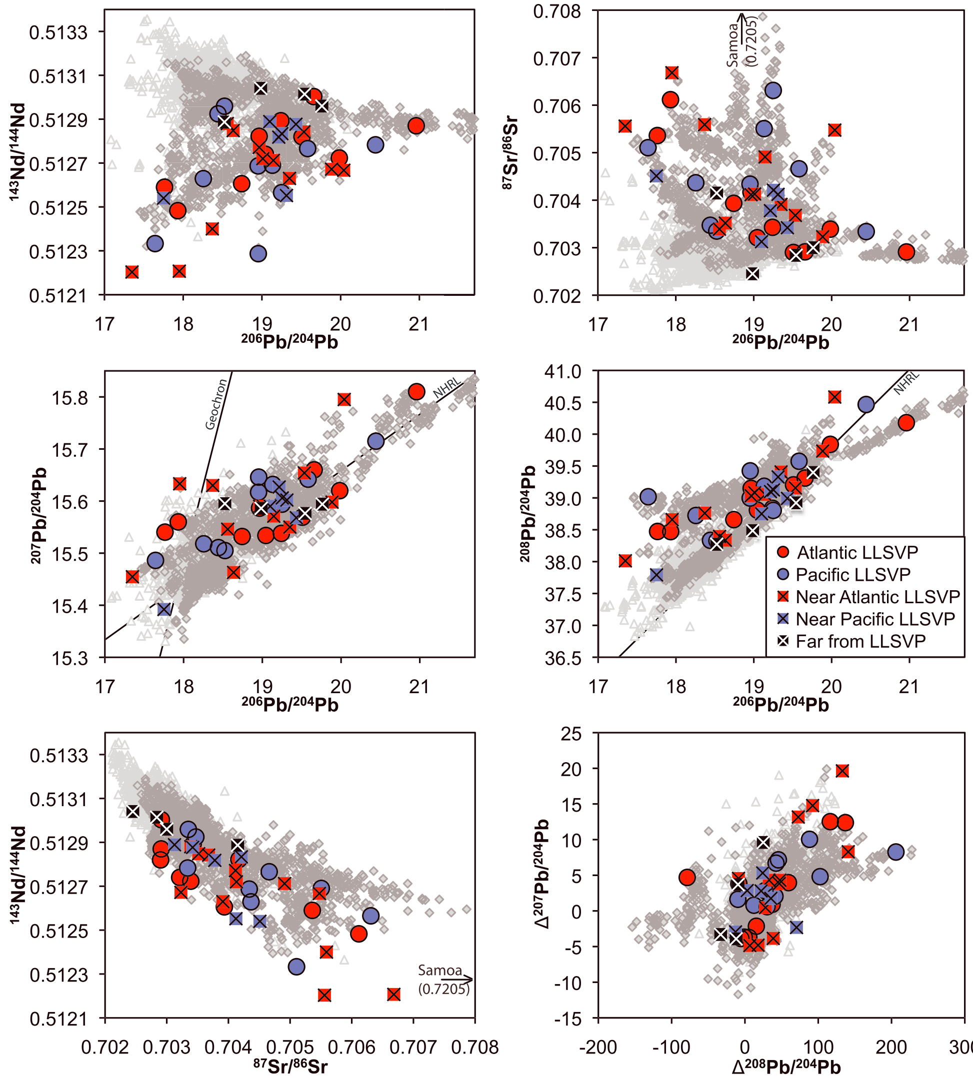

Figure 4. Radiogenic isotopic compositions for oceanic lavas with the lowest ^{143}Nd/^{144}Nd from 42 geochemically characterized oceanic hot spots. Global MORB (light gray symbols) and ocean island basalt (dark gray symbols) lavas are shown for reference. The NHRL (Northern Hemisphere reference line) is from Hart (1984). All values are shown in supporting information Table S1. The SMEAN2 composite tomography model is used to define the large low shear wave velocity province (LLSVP) margins, as discussed in the text, and is used to define hot spots as LLSVP hot spots, near-LLSV hot spots, or far from LLSVP hot spots. Hot spots geographically associated with the Atlantic (red symbols) and Pacific (blue symbols) LLSVPs exhibit considerable compositional overlap, and it is not clear that the two LLSVPs exhibit resolvable differences in their enriched mantle compositions.

3.1. Distribution of Extreme EM and HIMU Compositions at Oceanic Hotspots as a Function of Longitude

3.1.1. EM Components as a Function of Longitude

Figure 6 shows the minimum ^{143}Nd/^{144}Nd for each of the 42 oceanic hot spots as a function of the longitude of the current location of each hot spot (see Table 1). This figure facilitates comparison of the range of the most geochemically enriched compositions sampled by oceanic hot spots from the two LLSVPs. A first-order observation is that there is no relationship between longitude and the most geochemically enriched lavas from global oceanic hot spots.

All 13 oceanic hot spots with geochemically enriched ^{143}Nd/^{144}Nd (i.e., ^{143}Nd/^{144}Nd $\leq$ 0.512630; Bouvier et al., 2008) are either LLSVP or near-LLSVP hot spots: Six of the hot spots with geochemically enriched Nd-isotopic compositions are geographically associated with the Pacific LLSVP and seven with the Atlantic LLSVP. All four

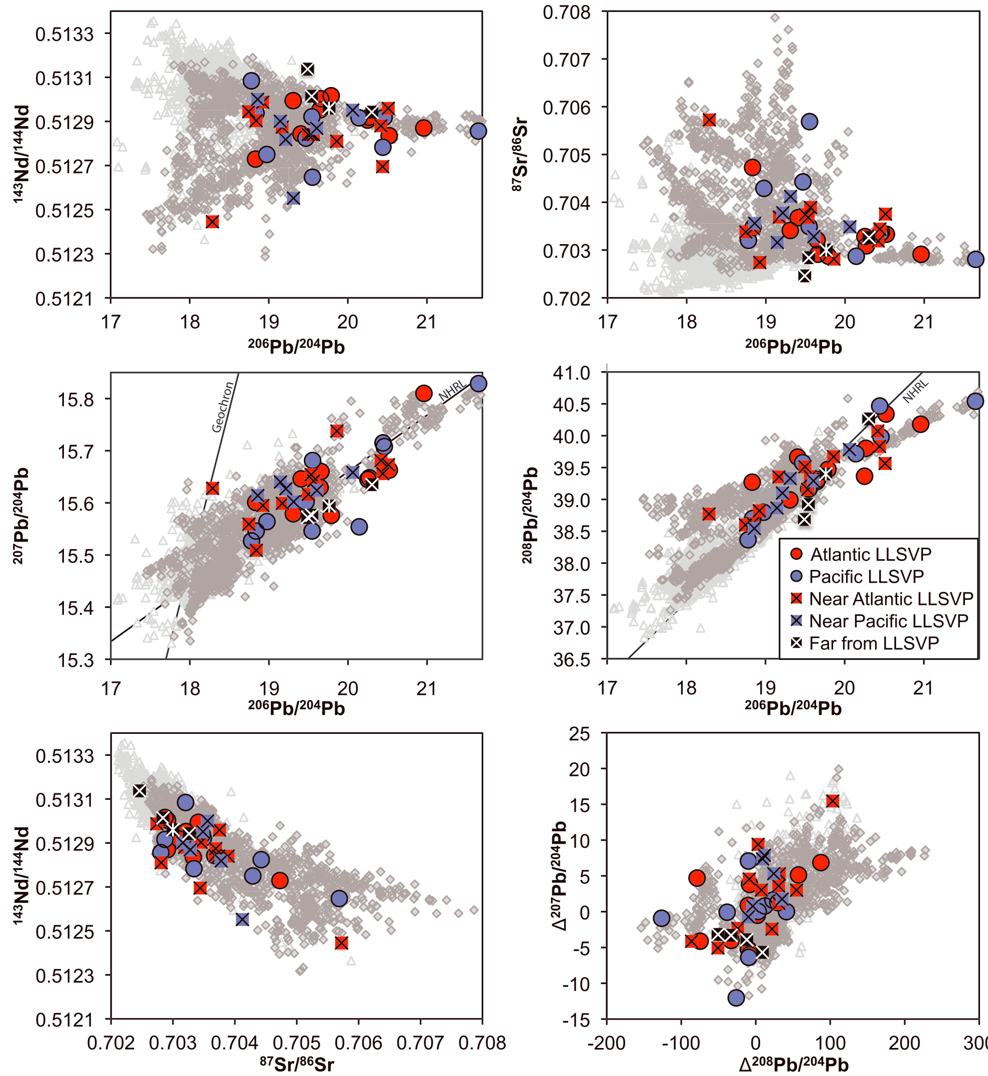

Figure 5. Radiogenic isotopic compositions for oceanic lavas with the highest $^{206}Pb/^{204}Pb$ from 42 geochemically characterized oceanic hot spots. Global MORB (light gray symbols) and ocean island basalt (dark gray symbols) lavas are shown for reference. The NHRL (Northern Hemisphere reference line) is from Hart (1984). All values are shown in supporting information Table S2. The SMEAN2 composite tomography model is used to define the large low shear wave velocity province (LLSVP) margins, as discussed in the text, and is used to define hot spots as LLSVP hot spots, near-LLSV hot spots, or far from LLSVP hot spots. Hot spots geographically associated with the Atlantic (red symbols) and Pacific (blue symbols) LLSVPs exhibit considerable compositional overlap.

oceanic hot spots located far from the LLSVPs—Balleny, Cobb-Axial-Juan de Fuca, Bowie-Pratt Welker, and Baja-Guadalupe—exhibit only non-EM compositions, and there is no evidence that enriched mantle domains are sampled by hot spots farthest from the LLSVP margins. Another key observation is that while all 13 of the oceanic hot spots with geochemically enriched $^{143}Nd/^{144}Nd$ are LLSVP and near-LLSVP hot spots, most (25 out of 38) LLSVP and near-LLSVP oceanic hot spots exhibit only non-EM $^{143}Nd/^{144}Nd$: 15 hot spots geographically associated with the Atlantic LLSVP and 10 hot spots associated with the Pacific LLSVP have $^{143}Nd/^{144}Nd > 0.512630$ (Table 1). Additionally, oceanic hot spots associated with the Atlantic LLSVP do not sample substantially more extreme enriched mantle compositions than hot spots geographically associated with the Pacific LLSVP: While two Atlantic hot spots have the lowest $^{143}Nd/^{144}Nd$ in the global oceanic hot spot database (Tristan-Gough and Discovery hot spots have minimum $^{143}Nd/^{144}Nd$ values of 0.512203 and 0.512207, respectively), two Pacific hot spots have the third and fourth lowest $^{143}Nd/^{144}Nd$ among oceanic hot spots (Samoa and Pitcairn have values of 0.512287 and

10.1029/2018GC007552

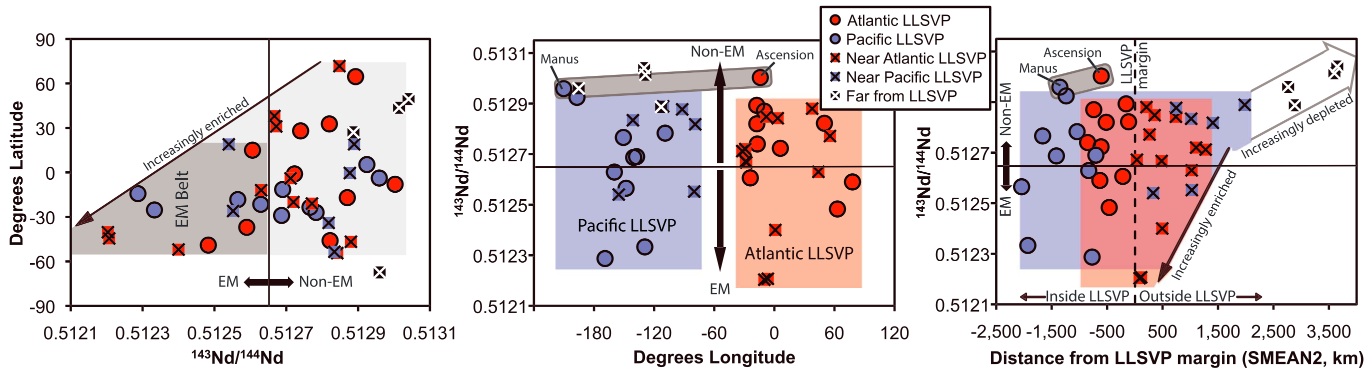

Figure 6. The minimum $^{143}Nd/^{144}Nd$ at each of 42 oceanic hot spots is shown as a function of latitude (left panel), longitude (middle panel), and distance from the large low shear wave velocity province (LLSVP) margins (right panel). Negative distances reflect hot spots located inside the LLSVP margins, and positive distances represent hot spots located outside of the LLSVPs; distances are defined as the minimum distance from a hot spot to the LLSVP margin (using the 75% of RMS velocity contour at 2,875-km depth in the SMEAN2 seismic model). The left panel shows that oceanic hot spots with the most extreme enriched mantle (EM) ($^{143}Nd/^{144}Nd < 0.5125$) compositions are found only in the Southern Hemisphere. The middle panel shows that hot spots at both LLSVPs exhibit a similar range of minimum $^{143}Nd/^{144}Nd$ compositions and indicate that neither LLSVP has a greater tendency to sample extreme EM compositions. The right panel shows that while hot spots located inside the LLSVPs host a range of minimum $^{143}Nd/^{144}Nd$ compositions, the appearance of the most EM (lowest $^{143}Nd/^{144}Nd$) hot spots is less common with increasing distance outside of the LLSVP margins, and only non-EM (geochemically depleted) hot spots are found at the greatest distances outside of the LLSVP margins. Manus Basin and Ascension hot spots have the least enriched components among the oceanic hot spots, which may owe to these hot spots being centered on a back arc spreading center and a mid-ocean ridge, respectively; these two hot spots are shown separately in some panels because their compositions may reflect a contribution from the depleted upper mantle. Supporting information Figure S1 shows the panels of this figure but uses the Lekic et al. (2012) seismic model to define the LLSVP margins for purposes of hot spot classification.

0.512333, respectively; Figure 3). Lastly, the Atlantic LLSVP hot spot with the least enriched minimum $^{143}Nd/^{144}Nd$ composition (0.513003, Ascension) is not significantly more depleted than the Pacific hot spot with the least enriched $^{143}Nd/^{144}Nd$ (0.512959, Manus Basin), but both oceanic hot spots are ridge centered and the high $^{143}Nd/^{144}Nd$ may reflect a contribution from the depleted upper mantle source of ridges. All of these observations hold for both the SMEAN2 (Figure 6) and the Lekic et al. (2012; supporting information Figure S1) based approaches for determining LLSVP boundaries.

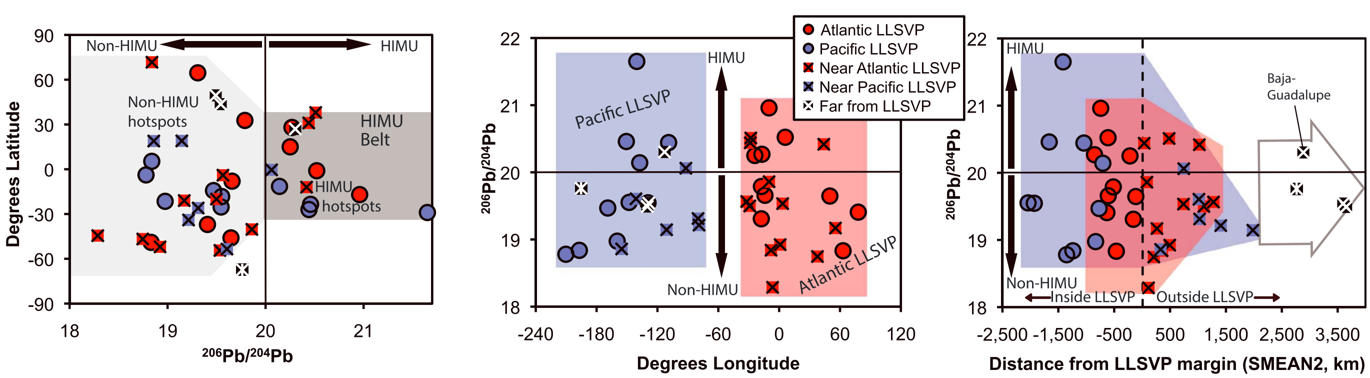

Figure 7. The maximum $^{206}Pb/^{204}Pb$ at each of 42 oceanic hot spots is shown as a function of latitude (left panel), longitude (middle panel), and distance from the LLSVP margins (right panel). Negative distances reflect hot spots located inside the LLSVP margins, and positive distances represent hot spots located outside of the LLSVPs; distances are defined as the minimum distance from a hot spot to the LLSVP margin (using the 75% of RMS velocity contour at 2,875-km depth in the SMEAN2 composite tomography model). The left panel shows that the most extreme HIMU (highest $^{206}Pb/^{204}Pb$) compositions at oceanic hot spots are concentrated near the tropical latitudes, and HIMU hot spots are absent at high latitudes. Unlike the EM component, which is expressed most strongly in southern hemisphere hot spots (see right panel), the HIMU component does not exhibit strong asymmetry between the Northern and Southern Hemispheres. While the HIMU domain is not clearly geographically associated with the LLSVPs, the middle panel shows that hot spots near both LLSVPs exhibit a similar range of maximum $^{206}Pb/^{204}Pb$ compositions, which indicates that neither region has a greater tendency to sample extreme HIMU compositions. The right panel shows that while hot spots located inside the LLSVPs host a range of maximum $^{206}Pb/^{204}Pb$ compositions, including the most extreme HIMU compositions (Macdonald and St. Helena hot spots), HIMU compositions are also found far outside of the LLSVP boundaries at the Baja-Guadalupe hot spot ($^{206}Pb/^{204}Pb = 20.3$); this panel also shows that there is not a clear relationship between magnitude of the HIMU signature at hot spots and distance from the LLSVP margins. In the right panel, the large arrow pointing to the right indicates that hotspots far from LLSVPs appear to have HIMU compositions. Supporting information Figure S2 shows the panels of this figure but uses the Lekic et al. (2012) seismic model to define the LLSVP margins for purposes of hot spot classification. EM = enriched mantle; HIMU = high $\mu = ^{238}U/^{204}Pb$; LLSVP = large low shear wave velocity province.

3.1.2. HIMU Mantle Components as a Function of Longitude

Oceanic hot spots located above or near the margins of the Atlantic LLSVP have a similar range in maximum $^{206}Pb/^{204}Pb$ compositions as the Pacific LLSVP and near-LLSVP hot spots (Figure 3). A hot spot located above Pacific LLSVP has the highest $^{206}Pb/^{204}Pb$ (Macdonald hot spot, $^{206}Pb/^{204}Pb = 21.65$ at the island of Mangaia) among global oceanic hot spots, and a hot spot located above the Atlantic LLSVP has the second highest maximum $^{206}Pb/^{204}Pb$ (St. Helena, $^{206}Pb/^{204}Pb = 20.96$). More oceanic hot spots with HIMU signatures (i.e., $^{206}Pb/^{204}Pb \geq 20$) are geographically associated with the Atlantic LLSVP ($N = 7$) than the Pacific LLSVP ($N = 5$; and one HIMU hot spot—Baja-Guadalupe—is located far from the LLSVPs). A key observation is that the range of maximum $^{206}Pb/^{204}Pb$ values at oceanic hot spots associated with the Atlantic LLSVP is similar to that of the Pacific LLSVP hot spots, and neither LLSVP shows a greater tendency to sample HIMU compositions. This observation again holds true across both seismic models for the LLSVPs considered here (Figures 7 and S2 in the supporting information).

Figure 7 shows the maximum $^{206}Pb/^{204}Pb$ compositions of all 42 oceanic hot spots as a function of longitude and reveals no global relationships between longitude and the most HIMU compositions from global oceanic hot spots. The figure also shows that most LLSVP and near-LLSVP oceanic hot spots (26 out of 38, or ~68%) lack highly radiogenic Pb (i.e., $^{206}Pb/^{204}Pb < 20$) and thus fail to exhibit HIMU signatures: 15 of these oceanic hot spots are geographically associated with the Atlantic LLSVP and 11 oceanic hot spots with the Pacific LLSVP have $^{206}Pb/^{204}Pb < 20$.

While all oceanic hot spots sampling the enriched mantle ($^{143}Nd/^{144}Nd \leq 0.512630$) domains are LLSVP or near-LLSVP hot spots (and none are located far from the LLSVPs), one of the 13 hot spots with a HIMU signature ($^{206}Pb/^{204}Pb \geq 20$) in the database of oceanic hot spots is among the group of four hot spots located farthest from the LLSVPs (see histogram in Figure 1). Situated ~2,885 km from the Pacific LLSVP margin in the SMEAN2 model, the Baja-Guadalupe hot spot has $^{206}Pb/^{204}Pb$ ratios of up to 20.3. The presence of radiogenic Pb-isotopic signatures in the Baja-Guadalupe hot spot suggests that HIMU signatures can be found in the oceanic mantle far from the LLSVP margins. This observation also holds for the Lekic et al. (2012)-derived set, in which Baja-Guadalupe is one of the four hot spots located farthest from the LLSVPs (see supporting information Figure S2).

If the threshold value for HIMU hot spots is increased to $^{206}Pb/^{204}Pb \geq 20.4$ to exclude Baja-Guadalupe, only eight hot spots qualify as HIMU, and all of them are geographically associated with the LLSVPs. However, the relationship (if any) between maximum $^{206}Pb/^{204}Pb$ at oceanic hot spots and distance from the LLSVP margin is unclear (see section 3.3).

3.2. Distribution of Extreme EM and HIMU Components at Oceanic Hotspots as a Function of Latitude

3.2.1. Distribution of the Most Extreme EM Lavas at Oceanic Hotspots as a Function of Latitude

In Figure 6, the minimum $^{143}Nd/^{144}Nd$ ratios identified at each of the 42 oceanic hot spots are plotted as a function of the latitude of the current hot spot location. We find that all 13 oceanic hot spots that sample geochemically enriched Nd-isotopic mantle domains (i.e., $^{143}Nd/^{144}Nd \leq 0.512630$) are located south of 19°N latitude, and 11 of the 13 EM hot spots are in the Southern Hemisphere. The six oceanic hot spots that sample the most extreme enriched domains ($^{143}Nd/^{144}Nd < 0.5125$)—Samoa, Pitcairn, Heard, Tristan-Gough, Discovery, and Meteor-Shona—are found exclusively in the Southern Hemisphere (south of 14°S; Figure 6). The observation of extreme geochemical enrichment in Southern Hemisphere oceanic hot spots, but not in northern hemisphere oceanic hot spots, confirms earlier observations of the geochemically enriched DUPAL anomaly in the Southern Hemisphere (Hart, 1984, 1988). This geographic "EM belt" is defined by oceanic hot spots with geochemically enriched $^{143}Nd/^{144}Nd$ (≤ 0.512630) and is found from 19°N (Hawaii) to 52°S (Meteor-Shona). The "extreme EM belt" (including only hotspots with $^{143}Nd/^{144}Nd < 0.5125$) is located south of 14°S.

We evaluate the significance of the observation that all 13 EM hot spots ($^{143}Nd/^{144}Nd \leq 0.512630$) are located between 18.9°N and 52°S, a region that encompasses 56% of the Earth's surface. If the distribution of EM hot spots at the Earth's surface is random, then the probability of all 13 EM hot spots being located in an area that encompasses just over half of Earth's surface area is only 0.053% ($p = 0.56^{13}$). Similarly, the six most extreme EM ($^{143}Nd/^{144}Nd < 0.5125$) hot spots, located between 14.3°S and 52°S, lie within 27.1% of Earth's surface area. Again, if one assumes that the distribution of extreme EM hot spots at the Earth's surface is random, then the probability of having all six extreme EM hot spots being clustered in such a small fraction of

Earth's surface is 0.039%. In this sense, the clustering of EM hot spots in a narrow range of latitudes, and the clustering of the extreme EM hot spots within an even narrower range of latitudes, is highly significant.

While EM hot spots are primarily concentrated in the Southern Hemisphere, not all southern hemisphere oceanic hot spots are geochemically enriched. In the oceanic hot spot database examined here, hot spots that source only non-EM compositions ($^{143}Nd/^{144}Nd > 0.512630$) are observed at *all* latitudes, including the Southern Hemisphere: Figure 6 shows that 18 out of the 29 (or ~62%) Southern Hemisphere oceanic hot spots sample only non-EM compositions (i.e., $^{143}Nd/^{144}Nd > 0.512630$). By comparison, 11 out of the 13 (or ~85%) Northern Hemisphere oceanic hot spots exhibit only non-EM $^{143}Nd/^{144}Nd$.

3.2.2. Distribution of the Most Extreme HIMU Lavas at Oceanic Hotspots as a Function of Latitude

The lavas with the highest $^{206}Pb/^{204}Pb$ from each of the 42 geochemically characterized oceanic hot spots are plotted as a function of latitude in Figure 7. While oceanic hot spots with the most geochemically enriched compositions (lowest $^{143}Nd/^{144}Nd$) are concentrated in the southern hemisphere, hot spots with the most extreme HIMU ($^{206}Pb/^{204}Pb \geq 20$) do not show a clear bias to the southern hemisphere. The two highest $^{206}Pb/^{204}Pb$ oceanic hot spots—St. Helena ($^{206}Pb/^{204}Pb = 20.96$) and Macdonald (21.65)—are located in the Southern Hemisphere, and 8 out of the 13 (or ~62%) HIMU hot spots are in the Southern Hemisphere. However, the lower proportion of HIMU oceanic hot spots in the Northern Hemisphere compared to the Southern Hemisphere may relate to the fact that there are fewer total Northern Hemisphere oceanic hot spots (13 out of 42, or ~31%) than Southern Hemisphere oceanic hot spots (29 out of 42, or ~69%) in our database. There is no evidence that the HIMU domain is concentrated in the Southern Hemisphere.

Instead, HIMU oceanic hot spots are found within a globe-encircling belt that is located near the Northern and Southern Hemisphere tropical latitudes (Figure 7). We refer to the higher concentration of HIMU oceanic hot spots near the tropical latitudes as the "HIMU belt". Here we define the HIMU belt geographically as the range of latitudes where oceanic hot spots with $^{206}Pb/^{204}Nd \geq 20$ are found (i.e., from 38°N (Azores) to 29°S (Macdonald)).

We assume that the distribution of HIMU hot spots on the Earth's surface is random in order to calculate the probability that all 13 HIMU hot spots are located between 38°N and 29°S. Because this range of latitudes encompasses just 55% of the Earth's surface, the probability of this occurring is 0.042%, which indicates that the clustering of the 13 HIMU hot spots between a narrow range of latitudes is highly significant. We also use existing hot spot locations of the 42 hot spots to calculate the probability that HIMU compositions are found only between 38°N and 29°S. In this simulation, we assume that the distribution of HIMU compositions at hot spots (but not hot spot locations) is random. We find that the probability of having all the HIMU-flavored hot spots between 38°N and 29° S is still only 0.1%, which again points to the significance of the clustering of HIMU hot spots near the tropics.

Oceanic hot spots that exhibit only unradiogenic Pb are found at all latitudes, including the HIMU belt near the tropical latitudes, where the non-HIMU hot spots ($^{206}Pb/^{204}Pb < 20$) are interspersed with hot spots that have HIMU signatures. In fact, 14 oceanic hot spots with non-HIMU signatures are found in the HIMU belt between 38°N and 29°S (i.e., the range of latitudes where all 13 HIMU hot spots are found), and 15 non-HIMU oceanic hot spots are found outside of this range of latitudes.

3.3. Distribution of Extreme EM and HIMU Components in Oceanic Hotspots as a Function of Distance From the LLSVP Margins

3.3.1. Distribution of the Most Extreme EM Lavas in Oceanic Hotspots as a Function of Distance From the LLSVPs

The minimum $^{143}Nd/^{144}Nd$ at each oceanic hot spot is shown as a function of distance from the nearest LLSVP in Figure 6, and this figure helps to evaluate whether geochemical enrichment at oceanic hot spots varies as a function of distance from the LLSVPs. Oceanic hot spots that lie within the LLSVP boundaries exhibit a wide range of minimum $^{143}Nd/^{144}Nd$ values, from EM to non-EM compositions. However, with increasing distance outside of the LLSVPs, the variability in $^{143}Nd/^{144}Nd$ decreases. Furthermore, oceanic hot spots exhibit a monotonically increasing lower limit on the $^{143}Nd/^{144}Nd$ ratios with increasing distance from the LLSVP margins (as highlighted by the arrows in Figure 6). The four oceanic hot spots located farthest from the LLSVPs—Balleny, Baja-Guadalupe, Cobb-Axial-Juan de Fuca, and Bowie-Pratt Welker—sample only non-EM compositions. If two ridge-centered hot spots with unusually high $^{143}Nd/^{144}Nd$—Ascension and Manus—are removed from consideration (owing to a possible contribution from the geochemically depleted upper mantle), the difference between LLSVP-associated oceanic hot spots and oceanic hot spots located far from the LLSVPs is made clearer: three of the four non-LLSVP (i.e., far from LLSVP) hot spots have higher $^{143}Nd/^{144}Nd$ than the LLSVP and near-LLSVP hot spots. In summary, while oceanic hot spots located inside the LLSVPs host both geochemically enriched (EM) and depleted (non-EM) Nd-isotopic compositions, the appearance of the most EM (lowest $^{143}Nd/^{144}Nd$) oceanic hot spots is less common with increasing distance outside of the LLSVP margins, and only non-EM oceanic hot spots are found far from the LLSVP margins. These observations hold for the LLSVPs defined in the SMEAN2 and Lekic et al. (2012) models (Figures 6 and S1 in the supporting information).

3.3.2. Distribution of the Most Extreme HIMU Lavas at Oceanic Hotspots as a Function of Distance From the LLSVPs

While the presence of geochemical enrichment (i.e., low $^{143}Nd/^{144}Nd$) in oceanic hot spots appears to relate to distance from the margins of an LLSVP, a relationship between the magnitude of hot spot HIMU signatures (i.e., maximum $^{206}Pb/^{204}Pb$) and distance from the margin of the LLSVPs is less clear. One observation is that the variability in maximum $^{206}Pb/^{204}Pb$ ratios is greater within the LLSVPs, and the variability diminishes with increasing distance from the LLSVP margins. However, this observation is biased by the two hot spots with the most extreme HIMU compositions among oceanic hot spots globally—Macdonald and St. Helena—which are located inside of the LLSVP margins. After excluding the Macdonald and St. Helena hot spots, the remaining 40 oceanic hot spots exhibit a similar range of $^{206}Pb/^{204}Pb$ (irrespective of distance from the LLSVP margins in the SMEAN2 seismic model), and the magnitude of the HIMU signature at oceanic hot spots does not show a clear reduction with distance outside of the LLSVPs (Figure 7). Indeed, the presence of a HIMU signature at Baja-Guadalupe, located 2,885 km from the LLSVP boundary in the SMEAN2 model, suggests that strong HIMU signatures are not limited to oceanic hot spots within or near the LLSVP boundaries in the same way that EM signatures at oceanic hot spots are. These observations hold for both of the seismic models examined here (Figures 7 and S2 in the supporting information).

4. Discussion

4.1. Similar Range of Compositions in Atlantic and Pacific LLSVP Oceanic Hotspots: Evidence for a Similar History of Formation and Evolution

Comparison of the radiogenic isotopic compositions of the oceanic hot spot lavas erupted above the two LLSVPs can provide clues about whether the two provinces share similar, or different, histories of formation and geochemical evolution. One question is whether observed seismic differences between the two LLSVPs is indicative of significant differences in their compositional makeup. Seismological and geodynamic studies have suggested different morphologies for the two LLSVPs: while the Pacific LLSVP has an oval shape and the long axis extends in an east-west direction, the Atlantic LLSVP is elongated in a north-south direction and has a "peninsula" in the southernmost portion that extends to the east under the Indian ocean (e.g., Garnero et al., 2016; Masters et al., 2000; McNamara & Zhong, 2005). Garnero et al. (2016) review growing evidence for seismic heterogeneity within the LLSVPs, including isolated structures within the Pacific LLSVP (He & Wen, 2012), smaller-scale structures (1–10 km) within the LLSVPs that cause seismic scattering (Rost et al., 2015), and ultra-low velocity zones identified within both LLSVPs (e.g., McNamara et al., 2010; Yu & Garnero, 2018). These observations have been interpreted to be consistent with substantial compositional and/or structural heterogeneity within the LLSVPs, and Garnero et al. (2016) suggested that "compositional difference [s] between the two LLVPs cannot be ruled out" (LLVP signifies large low velocity province, as *P* waves also show low velocity anomalies in the LLSVPs).

However, we find that oceanic hot spots above the two LLSVPs have similar ranges of extreme EM compositions (Figures 3–7). It is not known whether the LLSVPs are primordial features (it is also suggested that primordial domains exist elsewhere in the mantle; Ballmer et al., 2017; Becker et al., 1999) or were formed by accumulation of subducted material over geologic time, or both (e.g., Brandenburg & van Keken, 2007; Coltice et al., 2011; Garnero et al., 2016; Hirose et al., 1999; Jellinek & Manga, 2004; Knittle & Jeanloz, 1989; Kramers & Hofmann, 2006; Labrosse et al., 2007; Lee et al., 2010; McNamara & Zhong, 2004; Mulyukova et al., 2015; Mundl et al., 2017; Mukhopadhyay, 2012; Tackley, 1998, 2000, 2002). Nonetheless, the similarities in the range of extreme EM compositions in oceanic hot spots over the LLSVPs suggest that both have had broadly similar modes and histories of formation and evolution. If EM mantle compositions are formed by subduction of continentally derived materials (crust and sediment; e.g., Hofmann, 1997; White & Hofmann, 1982; Zindler & Hart, 1986), then one possible explanation for the similar range of EM compositions at oceanic hot spots that are geographically associated with the two LLSVPs is that similar quantities of similarly processed (in subduction zones) lithologies of subducted materials were added to LLSVPs over a similar time period. If differentially (subduction zone) processed, heterogeneous sediments and crust (with different final parent-daughter ratios, e.g., Sm/Nd) were added to the two LLSVPs at different times, the extreme EM compositions in the two LLSVPs would evolve different radiogenic isotopic compositions, which is not observed.

Alternatively, the similarity in extreme EM compositions sampled by the two LLSVPs might result if these two provinces periodically merge and then pull part (e.g., Zhong et al., 2007). If the LLSVPs merge, there exists the potential for "communication" via mass exchange between the provinces, which could help maintain a similar range of extreme EM compositions that are sampled by oceanic hot spots associated with the two LLSVPs. The similar range of geochemical extreme compositions provides a key constraint that suggests a similar origin and history of, or periodic mass exchange between, the LLSVPs.

While the HIMU hot spots that are geographically associated with the Pacific LLSVP exhibit a similar range of compositions as HIMU hot spots associated with the Atlantic-Indian LLSVP, the lack of a clear relationship between HIMU compositions at hot spots and their distances from the LLSVPs (e.g., Figure 7 and section 3.3.2) makes it difficult to argue that the HIMU domain is located within the LLSVPs. Therefore, we do not use the similar range of HIMU compositions at hot spots in the region of both LLSVPs to argue for a similar history and origin.

4.2. Geographic Relationships Between LLSVP Locations and EM and HIMU Components at Oceanic Hotspots

Jackson et al. (2018) found that oceanic hot spots not sourced by plumes (which sample only the upper mantle) are less likely to host extreme EM and HIMU compositions than hot spots associated with seismically constrained mantle plumes (which originate in the deep mantle). This observation supports a model where the extreme EM and HIMU domains are located *deeper* in the mantle than the depleted upper mantle sampled by MORB and nonplume hot spots (Jackson et al., 2018). Here we evaluate whether the geochemically extreme signatures sampled by oceanic hot spots are geographically associated with (i.e., lie above or near the margins of) the Atlantic and Pacific LLSVPs. Such an association, if observed, would support the hypothesis that geochemically extreme mantle domains are concentrated in the LLSVPs.

4.2.1. All EM Oceanic Hotspots Are Geographically Associated With the LLSVPs (But Most LLSVP Oceanic Hotspots Lack EM Signatures)

The geographic coincidence of EM oceanic hot spots and the LLSVPs, together with the observation that EM oceanic hot spots show an association with mantle plumes (Jackson et al., 2018), supports a model where the LLSVPs host EM domains that are entrained by upwelling plumes that feed hot spots overlying the LLSVPs. The lack of enriched mantle material in oceanic hot spots farthest from the LLSVPs (Figure 6) suggests that enriched mantle material is not located in the mantle far from the margins of the LLSVPs.

There are five oceanic hot spots with EM $^{143}Nd/^{144}Nd$ compositions that are located relatively close to, but just outside of, the LLSVP margins of the SMEAN2 model: Tristan-Gough (minimum $^{143}Nd/^{144}Nd$ is 0.512203, and the hot spot is located 85 km from the LLSVP margin), Discovery (0.512231, 114 km), Meteor-Shona (0.512400, 494 km), Hawaii (0.512540, 331 km), and San Felix (0.512552, 1028 km). However, the positioning of these oceanic hot spots outside of the LLSVPs may be due to uncertainties in (1) the locations of the actual boundaries of the LLSVPs (resulting from the choice of a certain contour as boundary and uncertainties in the seismic models used to construct SMEAN2) or (2) the locations of the mantle plumes. Thus, plumes sourcing these five hot spots may actually be rooted in the LLSVPs.

While there is a strong geographic association between the presence of extreme EM signatures at oceanic hot spots and their location above (or near the margins of) the LLSVPs, there is a wrinkle in the relationship: not all oceanic hot spots that are geographically associated with the LLSVPs exhibit EM compositions. An important question is why some oceanic hot spots that are geographically associated with the LLSVPs exhibit EM signatures, but other hot spots that are associated with the LLSVPs do not.

The lack of EM signatures in some oceanic hot spots that overlie the LLSVPs is unlikely to relate to undersampling. For example, the Canary and Iceland hot spots, both of which overlie the Atlantic LLSVP, have been extensively sampled and have yielded no evidence of lavas with EM $^{143}Nd/^{144}Nd$ compositions. One explanation for the lack of EM signatures in hot spots located over the LLSVPs is purely thermal plumes that rise from the thermal boundary layer at the top or near the margins of the LLSVPs would entrain little or no LLSVP material. However, this explanation is not consistent with the observation that many of the non-EM plumes—including Canary and Iceland—are interpreted to be thermochemical plumes due to the apparent width of their conduits in seismic studies (e.g., French & Romanowicz, 2015) and are therefore likely to have entrained chemically heterogeneous material from the base of the mantle. Lastly, ambient upper mantle material entrained in upwelling plumes is unlikely to contribute to melting (Farnetani & Richards, 1995), so entrained ambient upper mantle is unlikely to contribute to these non-EM hot spots; instead, entrainment of ambient lower mantle material, at the base of the upwelling plume, is likely to dominate the material hosted in a plume (Ballmer et al., 2016). While we cannot rule out a shallow contribution to hot spot geochemistry due to uppermost mantle heterogeneities in the melting region of the plume, a range of observations are consistent with a deep origin (e.g., Castillo, 1988; Jackson et al., 2018), and we consider that the geographic association of EM hot spots and LLSVPs is compelling and likely not coincidence.

Therefore, we favor an alternative explanation for the origin of non-EM hot spots that are geographically associated with the LLSVPs. If hot spots geographically associated with the LLSVPs—like the Canary and Iceland hot spots—are fed by upwelling plumes that draw material from the LLSVPs, then the lack of EM signatures at these two hot spots suggests that non-EM domains exist in the LLSVPs, and some hot spots only entrain these domains. This is not difficult to accomplish from a conceptual standpoint, as it has long been thought that geochemically depleted (non-EM) domains exist in the deep mantle, and we prefer a model where geochemically depleted domains reside in the lower mantle and are entrained by upwelling plumes sourcing hot spots (Zindler & Hart, 1986). If oceanic hot spots *without* EM (all lavas have $^{143}Nd/^{144}Nd > 0.512630$) and *with* EM (at least one lava has $^{143}Nd/^{144}Nd \leq 0.512630$) signatures are sourced by the LLSVPs, an important conclusion is that the LLSVPs are isotopically heterogeneous, a conclusion supported by recent geodynamic models (Ballmer et al., 2016; Li et al., 2014).

4.2.2. HIMU Oceanic Hotspots Are Not Clearly Associated With LLSVPs

Unlike EM oceanic hot spots, which show a strong geographic association with the LLSVPs (Figure 6)—consistent with the hypothesis that EM oceanic hot spots derived their signatures from the LLSVPs—the geographic association between LLSVPs and HIMU ($^{206}Pb/^{204}Pb \geq 20$) oceanic hot spots is not as compelling (Figure 7; see section 3.3.2).

One reason for this is that one of the 13 HIMU oceanic hot spots—the Baja-Guadalupe hot spot—is located far from the LLSVPs in both seismic models considered here, which argues against the HIMU domain being strictly limited to the LLSVPs. As discussed in Jackson et al. (2018), the Baja-Guadalupe hot spot is not associated with a seismically detectable plume in any of the plume catalogues (Boschi et al., 2007; French & Romanowicz, 2015), which suggests that the HIMU domain sampled by Baja-Guadalupe is not necessarily limited to the lower mantle sampled by plumes but may reside in the upper mantle where it is sampled by nonplume hot spots like Baja-Guadalupe. However, we cannot exclude the possibility that a plume is located under Baja-Guadalupe that is undetectable with existing seismic techniques. If a mantle plume generated the volcanism at Baja-Guadalupe, then it can be argued that the HIMU signature sourcing this hot spot originated in the lower mantle. However, even if the HIMU signature in the Baja-Guadalupe hot spot was conveyed from the lower mantle, it is unlikely that the HIMU signature was sourced from the Pacific LLSVP owing to the large distance (2,885 km) from the LLSVP margin. Therefore, we cannot link the location of the Baja-Guadalupe HIMU domain in the mantle with the LLSVPs. Nonetheless, 12 of the 13 HIMU hot spots are geographically associated with the LLSVPs, so it is possible that a portion of the HIMU domain resides, at least in part, within the LLSVPs.

If a higher $^{206}Pb/^{204}Pb$ threshold for the HIMU component is chosen (where HIMU hot spots have $^{206}Pb/^{204}Pb \geq 20.4$), then all eight of these "extreme" HIMU hot spots—Macdonald, St. Helena, Cameroon,

10.1029/2018GC007552

Azores, Arago-Rurutu, Easter, Greater Meteor-New England, and Comores—are located over or near the margins of the LLSVPs. Again, however, the lack of a clear relationship between the magnitude of HIMU signatures at hot spots and their distances from the LLSVP margins argues against a HIMU "home" in the LLSVPs.

4.3. Distribution and Origin of EM and HIMU Domains in the Earth's Mantle

Recent numerical models suggest that both depleted and recycled domains can be intimately associated within the LLSVPs (Ballmer et al., 2016; Li et al., 2014; Nakagawa & Tackley, 2014). If hot spots overlying the LLSVPs are ultimately sourced by the LLSVPs, and if these reservoirs are proximally located within the LLSVPs, then it should not be surprising that both types of domains are sampled by lavas erupted at plume-fed hot spots (Williams et al., 2015). An important question is how recycled and depleted domains are distributed in the mantle.

The EM and HIMU reservoirs show clear geographic patterns in their distribution. A model that accurately describes the geographic distribution of EM and HIMU domains in the deep mantle must be consistent with several observations made in this paper. First, EM signatures ($^{143}Nd/^{144}Nd \leq 0.512630$) at oceanic hot spots are geographically associated with the LLSVPs (Figure 6), while oceanic hot spots with the most extreme HIMU signatures ($^{206}Pb/^{204}Pb \geq 20$) are not (Figure 7). Second, all oceanic hot spots with extreme EM signatures ($^{143}Nd/^{144}Nd < 0.5125$) are located entirely in the southern hemisphere (Figure 6), while HIMU oceanic hot spots are broadly centered near the tropical latitudes (Figure 7). Third, the magnitude of the most extreme EM (lowest $^{143}Nd/^{144}Nd$) signatures at oceanic hot spots diminishes monotonically from the Southern Hemisphere to the Northern Hemisphere high latitudes (Figure 6), while the magnitude of the most extreme HIMU signatures diminishes moving away from (i.e., north and south of) the tropical latitudes (Figure 7). Lastly, oceanic hot spots that host only non-HIMU ($^{206}Pb/^{204}Pb < 20$) or non-EM ($^{143}Nd/^{144}Nd > 0.512630$) are found at all latitudes. Below, we use observations of the global distributions of EM and HIMU signatures at oceanic hot spots to build a conceptual model for the distribution of EM and HIMU domains in the deep mantle (see Figure 8).

4.3.1. Distribution of EM and HIMU Domains

While the EM domain sampled by oceanic hot spots is shifted to the Southern Hemisphere, it is important to note that the enriched mantle signature of the EM geographic belt does not encompass the entire southern portions of the LLSVPs. This is because some Southern Hemisphere oceanic hot spots sample only non-EM compositions. One model consistent with this observation is that the southern portions of the LLSVPs contain EM plums (or "pockets") that are interspersed within a matrix of non-EM material that is sampled by Southern Hemisphere hot spots (Figure 8). In this way, some Southern Hemisphere plumes entrain plums of EM material, while other Southern Hemisphere plumes entrain only the non-EM LLSVP matrix, giving rise to both austral EM oceanic hot spots (i.e., hot spots that have at least one lava with $^{143}Nd/^{144}Nd \leq 0.512630$) and austral non-EM oceanic hot spots (i.e., hot spots that do not host any lavas with $^{143}Nd/^{144}Nd \leq 0.512630$). The paucity of EM oceanic hot spots in the Northern Hemisphere may owe to the EM plums being rarer in the Northern Hemisphere region of the LLSVPs (as illustrated in Figure 8), or to the EM plums exhibiting a geochemical gradient with latitude (such that EM plums exhibit less extreme signatures in the northerly latitudes compared to southern hemisphere EM plums, a model that is not shown in Figure 8). This way, stronger signatures of geochemical enrichment are transmitted via plumes to Southern Hemisphere oceanic hot spots that source the EM plums. However, we cannot exclude stratified compositional layering within the LLSVPs as a means of separating different deep mantle domains (e.g., EM vs non-EM) sourced by hot spots (Ballmer et al., 2016), but the EM material in this model would need to exhibit a latitudinal stratification to be consistent with the higher concentration of extreme EM hot spots in the Southern Hemisphere.

A similar "plum-in-the-LLSVP-matrix" model cannot be used to describe the distribution of HIMU domains in the LLSVPs because HIMU hot spots do not show the same clear geographic association with the LLSVPs that is seen with EM hot spots. However, unlike EM oceanic hot spots (which are concentrated in the southern hemisphere), HIMU oceanic hot spots are found primarily near the tropical latitudes, but like EM oceanic hot spots, oceanic hot spots with HIMU signatures ($^{206}Pb/^{204}Pb \geq 20$) are interspersed with nonextreme (non-HIMU) hot spots at the same latitudes. The absence of HIMU hot spots in the high northerly and southerly latitudes may owe to a greater abundance of HIMU plums near the tropics—both inside and

10.1029/2018GC007552

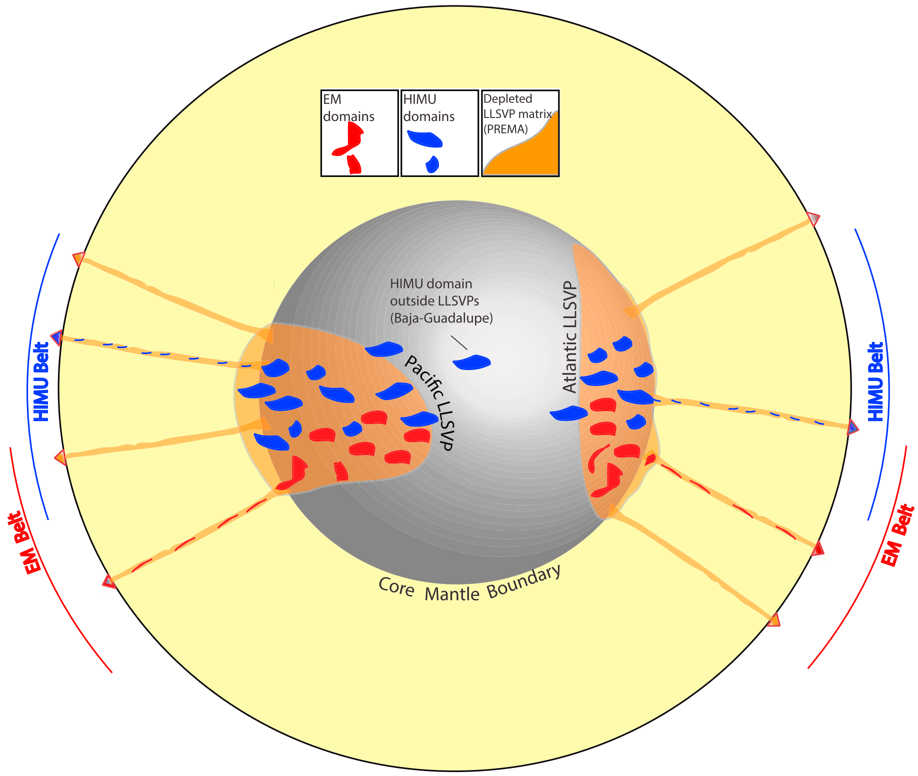

Figure 8. Cartoon illustrating the possible distribution of EM and HIMU components in the deep mantle. All hot spots with EM compositions ($^{143}Nd/^{144}Nd \leq 0.512630$) overlie the LLSVPs, and EM hot spots are observed primarily in the Southern Hemisphere (and the most extreme EM hot spots, with $^{143}Nd/^{144}Nd < 0.5125$, are limited entirely to the Southern Hemisphere). The geographic distribution of EM hot spots defines the geographic "EM belt". In the figure we assume that geochemically extreme components exist as plums in the deep mantle. The highest abundance of plums of extreme EM material (red blobs in LLSVPs), responsible for generating EM signatures at hot spots, is distributed in the southern hemispheric portions of the LLSVPs. In contrast, the most extreme HIMU compositions ($^{206}Pb/^{204}Pb \geq 20$) are observed within or near the tropical latitudes but are not necessarily associated with the LLSVPs. The geographic distribution of HIMU hot spots near the equator defines the HIMU geographic belt, and the highest abundance of plums of extreme HIMU material (blue blobs in figure) is distributed near the tropical latitudes of the Northern and Southern Hemispheres. The Baja-Guadalupe hot spot is an example of a HIMU hot spot located far from the LLSVP margins, indicating that the HIMU domains sampled by hot spots are not necessarily associated geographically with the LLSVPs. Therefore, in the figure, one HIMU pocket is located outside of the LLSVPs (and some HIMU pockets are displaced just outside of the LLSVPs) to indicate the lack of a clear association of the HIMU domain with the LLSVPs. The LLSVP matrix hosting EM and HIMU blobs is assumed to be PREMA in composition (i.e., non-EM and non-HIMU in composition). EM = enriched mantle; HIMU = high $\mu = {}^{238}U/^{204}Pb$; LLSVP = large low shear wave velocity province.

outside the LLSVPs—which enhances the likelihood of being sampled in the lower latitudes (as illustrated in Figure 8). Alternatively, the HIMU plums exhibit larger magnitude HIMU signatures near the tropics than any HIMU plums that might exist outside of the tropics (a model that is not shown in Figure 8). Because the HIMU domains are not geographically limited to the LLSVPs, as indicated by the presence of HIMU compositions at the Baja-Guadalupe hot spot located far from the LLSVP margins, plums of HIMU material are located both inside and outside of the LLSVPs and are concentrated near the tropical latitudes (Figure 8).

Existing geochemical evidence from oceanic hot spots does not support a model where the LLSVPs are primarily composed entirely of recycled EM or HIMU material, as this would be difficult to reconcile with the observations that (1) *most* hot spots geographically associated with the LLSVPs sample *only* non-EM or non-HIMU material and (2) the HIMU domain is not clearly linked to the LLSVPs. Furthermore, EM and HIMU compositions are generally rare even at the so-called EM and HIMU oceanic hot spots: most lavas erupted at EM and HIMU oceanic hot spots have non-EM $^{143}Nd/^{144}Nd$ ($^{143}Nd/^{144}Nd > 0.512630$) and non-HIMU $^{206}Pb/^{204}Pb$ ($^{206}Pb/^{204}Pb < 20$), respectively (Hart, 1988). These observations suggest that the bulk of the LLSVPs (i.e., the LLSVP "matrix" between the EM and HIMU plums) sampled by oceanic hot spots is composed of a non-EM and non-HIMU composition (Figure 8). Zindler and Hart (1986) found that the median Nd-isotopic composition at oceanic hot spots (approximately 0.5129 to 0.5130) is non-EM and is geochemically less depleted than (and therefore distinct from) the median Nd-isotopic composition of MORB, and they referred to this componentin OIBs as PREMA (Prevalent Mantle). This non-EM (geochemically depleted) mantle domain also has low $^{206}Pb/^{204}Pb$ (non-HIMU) compositions, is ubiquitously identified in plume-fed hot spots, and may reside in the lower mantle (Zindler & Hart, 1986). Given that most oceanic hot spots are situated over the LLSVPs (Figure 1), the abundance of geochemically depleted compositions at these hot spots may indicate that these are the dominant materials comprising the LLSVPs (i.e., the LLSVP matrix). A heterogeneous makeup of the LLSVPs is consistent with recent numerical models (Li et al., 2014; Williams et al., 2015).

The inferences about the distribution of recycled compositions in the mantle are true only if (1) hot spots overlying the LLSVPs are indeed fed by LLSVPs via upwelling plumes, (2) the array of recycled compositions sampled in hot spot lavas are representative of the compositions of the LLSVPs, and, (3) the geochemical distributions observed in oceanic hot spot lavas are not biased by other processes. It remains to be determined how or whether other processes—including dilution of entrained LLSVP material by greater entrainment of ambient lower mantle (i.e., non-LLSVP) material at the base of the plume during upwelling (Ballmer et al., 2016), preferential sampling of less dense deep mantle reservoirs relative to denser reservoirs (Jackson et al., 2017), and preferential melting of less refractory domains in plumes beneath hot spots (e.g., Ito & Mahoney, 2005a, 2005b; Ito & Mahoney, 2006)—complicate the approach of using the geochemistry of hot spot lavas to infer deep mantle compositions.

The last point is relevant because it is possible that basalts erupted at the surface are melts of a lithologically heterogeneous mantle, in which case the composition of erupted lavas may be controlled by the compositions and relative abundances of the different lithologies present in the mantle source. In this scenario, different lithologies yield heterogeneous melts that mix (Maclennan et al., 2003; Maclennan, 2008; Shorttle et al., 2014, 2016). As a result, basalt compositions may reflect aggregates of heterogeneous melts, and the true endmember compositions are not reflected in the final erupted basalts (Rudge et al., 2013; Stracke, 2012; Stracke & Bourdon, 2009). Nonetheless, the geographic association of EM hot spots with the LLSVPs suggests that spatial patterns in deep mantle sources, not shallow melting processes, play a dominant role in influencing the global distribution of EM compositions sampled at oceanic hot spots.

In future work, it will be important to consider whether plume strength varies depending on location with respect to the LLSVPs, and how this might influence entrainment of deep-seated domains. Due this uncertainty, we cannot exclude a model whereby EM domains are distributed ubiquitously in the lower mantle, but that plumes located outside of the LLSVPs are simply too weak (compared to plumes located inside the LLSVPs) to entrain deep EM domains. However, we do not find a relationship between hot spot buoyancy fluxes (from King & Adam, 2014) and the minimum $^{143}Nd/^{144}Nd$ at hot spots examined here, which argues against plume buoyancy controlling the magnitude of the EM signature observed at hot spots. A similar argument invoking "strong" versus weak plumes is unlikely to explain the preferential sampling of EM material in the southern portions of the LLSVPs relative to the northern regions. This is because the two plumes with among the highest hot spot buoyancy, Iceland and Hawaii (King & Adam, 2014), are located at the northern margins of the Atlantic and Pacific LLSVPs, respectively, yet Hawaii exhibits only a modest EM signature (lowest $^{143}Nd/^{144}Nd = 0.512540$) and Iceland exhibits no EM signature (lowest $^{143}Nd/^{144}Nd = 0.512893$).

4.3.2. Spatial Decoupling of the Geographic Distribution of EM and HIMU Domains in the Mantle

The spatial distributions of the EM and HIMU domains in the mantle, as sampled by oceanic hot spots, appear to be quite different: EM hot spots are located primarily over the southern hemispheric portions of the LLSVPs, while HIMU hot spots are concentrated primarily near the tropics and do not show a clear geographic relationship with the LLSVPs. It is not yet clear why the EM and HIMU domains are spatially decoupled in the mantle, but this may relate to different densities and/or viscosities of the EM and HIMU components, which may influence how they segregate or accumulate within the LLSVPs.

Furthermore, EM and HIMU domains are thought to form by subduction of continental and oceanic crust into the mantle over time. However, such subduction processes might be expected to generate random patterns in the distribution of EM and HIMU domains in the mantle (Hart, 1984). This makes the coherent pattern of the

10.1029/2018GC007552

Southern Hemisphere EM hot spots over the LLSVPs, and nonrandom clustering of HIMU hot spots near the tropical latitudes, even more perplexing. Whatever the mechanism responsible for generating the austral EM and tropical HIMU belts, if it relates to subduction, it is likely to have operated over long geologic timescales. Not only does deep subduction of oceanic lithosphere contribute the raw ingredients for formation EM and HIMU reservoirs (Hofmann & White, 1982; White & Hofmann, 1982) but also downgoing slabs may "push" lower mantle domains, thus guiding their locations (e.g., Zhang et al., 2010; Zhong et al., 2007) and the distributions of EM and HIMU domains in the deep Earth. If this is the case, subduction will ultimately determine the present-day composition *and* geographic distribution of the extreme EM and HIMU domains in the deep Earth. Chemical geodynamic models linking the geochemical evolution of the deep mantle (e.g., Brandenburg et al., 2008; Christensen & Hofmann, 1994; Nakagawa et al., 2010) with the input of downgoing slabs and their interaction with deep mantle reservoirs will provide key constraints on the origin of geographic patterns of EM and HIMU reservoirs in the mantle.

Subduction conveys heterogeneous material to the mantle over geologic time. If the EM domain is the result of subducted continentally derived crust, the strong geographic association of EM with the LLSVPs may suggest that these deep mantle domains are compositionally heterogeneous. An important task moving forward will be to deconvolve the chemical and thermal influences on the seismic properties of the LLSVPs.

5. Conclusions

We examine a geochemical compilation of extreme EM and HIMU compositions at 42 oceanic hot spots with published Sr, Nd, and Pb isotopic data on the same samples. The data provide new insights into the global distribution of EM and HIMU domains and their relationships with the LLSVPs.

1. EM domains show a clear geographic association with the LLSVPs: *all* 13 EM oceanic hot spots are geographically associated with LLSVPs. Furthermore, the magnitude of EM signatures (i.e., minimum $^{143}Nd/^{144}Nd$) in oceanic hot spots diminishes monotonically with increasing distance outside of the LLSVP margins, and oceanic hot spots located far from the LLSVPs lack EM signatures. The lack of mantle-derived lavas with EM signatures in oceanic hot spots farthest from the LLSVPs suggests that EM material is not located in the mantle far from the margins of the LLSVPs. The geographic coincidence of EM oceanic hot spots and the LLSVPs, together with the observation that EM oceanic hot spots show a geographic association with mantle plumes (Jackson et al., 2018), supports a model where the LLSVPs host EM domains that are entrained by upwelling plumes that feed hot spots overlying the LLSVPs.
2. In contrast, HIMU domains exhibit an imperfect geographic association with the LLSVPs: 12 of the 13 HIMU hot spots are located within or near the margins of the LLSVPs, but the presence of a HIMU signature at the Baja-Guadalupe hot spots (located far from the LLSVP margins) suggests that the HIMU domains are not necessarily linked with the LLSVPs. The total variability in maximum $^{206}Pb/^{204}Pb$ ratios at oceanic hot spots tends to be greater within the LLSVPs, diminishing with increasing distance from the LLSVP margins. However, unlike the EM component at hot spots, a relationship between the magnitude of hot spot HIMU signatures (i.e., maximum $^{206}Pb/^{204}Pb$) at oceanic hot spots and distance from the margin of the LLSVPs is unclear and does not support a hypothesis where HIMU domains are exclusively linked with the LLSVPs.
3. All oceanic hot spots with geochemically enriched $^{143}Nd/^{144}Nd$ exist within between 19°N and 52°S latitude and the most extreme EM oceanic hot spots ($^{143}Nd/^{144}Nd < 0.5125$) are concentrated in the Southern Hemispheric portions of the LLSVPs (14.3°S to 52°S), defining the "EM geographic belt" as a predominantly Southern Hemispheric feature. Oceanic hot spots hosting HIMU compositions show a different geographic distribution with latitude compared to EM hot spots, as HIMU hot spots are found primarily near the tropical latitudes of the LLSVPs, and we refer to this as the "HIMU geographic belt". These observations of latitudinal zonation of EM (Southern Hemisphere) and HIMU (near the tropical latitudes) domains are statistically significant, but the origin of (1) the EM and HIMU latitudinal zonation and (2) the decoupled spatial distribution of the EM and HIMU geographic belts is not known.
4. While EM and HIMU oceanic hot spots are concentrated in the Southern Hemisphere and near the tropical latitudes, respectively, we find that oceanic hot spots hosting only non-EM ($^{143}Nd/^{144}Nd > 0.512630$) or non-HIMU ($^{206}Pb/^{204}Pb < 20$) compositions are found at all latitudes. Furthermore, EM and HIMU compositions are rare in oceanic hot spots: most lavas erupted at oceanic hot spots, including the so-called EM

and HIMU hot spots, exhibit neither EM nor HIMU compositions. The median Nd-isotopic composition at oceanic hot spots is non-EM (geochemically depleted) and non-HIMU (low $^{206}Pb/^{204}Pb$; Zindler & Hart, 1986). This ubiquitous, geochemically depleted component in oceanic hot spot lavas, called PREMA, may reflect the dominant composition of the LLSVPs (i.e., the LLSVP matrix), and we infer that plums of EM domains are distributed within a geochemically depleted LLSVP matrix. In this model, EM plums are concentrated in the Southern Hemisphere geographic “EM belt” of the LLSVPs. HIMU plums are concentrated in the tropical HIMU geographic belt but are not necessarily limited to the LLSVPs.

5. We find that neither Atlantic-LLSVP oceanic hot spots nor Pacific-LLSVP oceanic hot spots exhibit a greater tendency to sample extreme EM compositions, and the range of extreme EM compositions is remarkably similar across the two LLSVPs. This is consistent with the hypothesis that the two LLSVPs formed by similar processes and have broadly similar histories, or that they merged periodically and exchanged material. However, because the HIMU domain is not necessarily limited to the LLSVPs, we do not use the similar range of HIMU compositions in oceanic hot spots geographically associated with the two LLSVPs to make inferences about LLSVP composition and history.

Acknowledgments

Reviews from Maxim Ballmer, Eric Brown, and two anonymous reviewers are acknowledged, as is editorial handling from Janne Blichert-Toft. MGJ acknowledges support from National Science Foundation EAR-1624840 and OCE-1736984, and TWB from EAR 1460479. Drew Reinhard is thanked for his help with Figures. We acknowledge the NSF-sponsored CIDER program for providing a venue for interdisciplinary collaboration, which made this project possible. All data used in this manuscript are presented in the Supplementary Tables.

References

Auer, L., Boschi, L., Becker, T. W., Nissen-Meyer, T., & Giardini, D. (2014). Savani: A variable-resolution whole-mantle model of anisotropic shear-velocity variations based on multiple datasets. *Journal of Geophysical Research: Solid Earth*, *119*, 3006–3034. https://doi.org/10.1002/2013JB010773

Austermann, J., Kaye, B. T., Mitrovica, J. X., & Huybers, P. (2014). A statistical analysis of the correlation between large igneous provinces and lower mantle seismic structure. *Geophysical Journal International*, *197*(1), 1–9. https://doi.org/10.1093/gji/ggt500

Ballmer, M. D., Houser, C., Hernlund, J. W., Wentzcovich, R., & Hirose, K. (2017). Persistence of strong silica-enriched domains in the Earth’s lower mantle. *Nature Geoscience*, *10*(3), 236–240. https://doi.org/10.1038/ngeo2898

Ballmer, M. D., Schumacher, L., Lekic, V., Thomas, C., & Ito, G. (2016). Compositional layering within the large low shear-wave velocity provinces in the lower mantle. *Geochemistry, Geophysics, Geosystems*, *17*, 5056–5077. https://doi.org/10.1002/2016GC006005

Becker, T. W., & Boschi, L. (2002). A comparison of tomographic and geodynamic mantle models. *Geochemistry, Geophysics, Geosystems*, *3*(1), 1003. https://doi.org/10.1029/2001GC000168

Becker, T. W., Kellogg, J. B., & O’Connell, R. J. (1999). Thermal constraints on the survival of primitive blobs in the lower mantle. *Earth and Planetary Science Letters*, *171*(3), 351–365. https://doi.org/10.1016/S0012-821X(99)00160-0

Boschi, L., Becker, T. W., & Steinberger, B. (2007). Mantle plumes: Dynamic models and seismic images. *Geochemistry, Geophysics, Geosystems*, *7*, Q10006. https://doi.org/10.1029/2007GC001733

Bouvier, A., Vervoort, J. D., & Patchett, P. J. (2008). The Lu–Hf and Sm–Nd isotopic composition of CHUR: Constraints from unequilibrated chondrites and implications for the bulk composition of terrestrial planets. *Earth and Planetary Science Letters*, *273*, 48–57.

Brandenburg, J. P., Hauri, E. K., van Keken, P. E., & Ballentine, C. J. A. (2008). Multiple system study of the geochemical evolution of the mantle with force-balanced plates and thermochemical effects. *Earth and Planetary Science Letters*, *276*, 1–13.

Brandenburg, J. P., & van Keken, P. E. (2007). Deep storage of oceanic crust in a vigorously convecting mantle. *Journal of Geophysical Research*, *112*, B06403. https://doi.org/10.1029/2006JB004813

Burke, K., Steinberger, B., Torsvik, T. H., & Smethurst, M. A. (2008). Plume generation zones at the margins of large low shear velocity provinces on the core–mantle boundary. *Earth and Planetary Science Letters*, *265*(1-2), 49–60. https://doi.org/10.1016/j.epsl.2007.09.042

Castillo, P. (1988). The DUPAL anomaly as a trace of the upwelling lower mantle. *Nature*, *336*(6200), 667–670. https://doi.org/10.1038/336667a0

Christensen, U. R., & Hofmann, A. W. (1994). Segregation of subducted oceanic crust in the convecting mantle. *Journal of Geophysical Research*, *99*, 19,867–19,884. https://doi.org/10.1029/93JB03403

Coltice, N., Moreira, M., Hernlund, J., & Labrosse, S. (2011). Crystallization of a basal magma ocean recorded by helium and Neon. *Earth and Planetary Science Letters*, *308*, 193–199.

Dupré, B., & Allègre, C. J. (1983). Pb–Sr isotope variation in Indian Ocean basalts and mixing phenomena. *Nature*, *303*(5913), 142–146. https://doi.org/10.1038/303142a0

Farnetani, D. G., & Richards, M. A. (1995). Thermal entrainment and melting in mantle plumes. *Earth and Planetary Science Letters*, *136*, 251–267.

French, S. W., & Romanowicz, B. (2015). Broad plumes rooted at the base of the Earth’s mantle beneath major hotspots. *Nature*, *525*(7567), 95–99. https://doi.org/10.1038/nature14876

Gale, A., Dalton, C. A., Langmuir, C. H., Su, Y., & Schilling, J.-G. (2013). The mean composition of ocean ridge basalts. *Geochemistry, Geophysics, Geosystems*, *14*, 489–518. https://doi.org/10.1029/2012GC004334

Garnero, E. J., McNamara, A. K., & Shim, S.-H. (2016). Continent-sized anomalous zones with low seismic velocity at the base of Earth’s mantle. *Nature Geoscience*, *9*(7), 481–489. https://doi.org/10.1038/ngeo2733

Hager, B. H., Clayton, R. W., Richards, M. A., Comer, R. P., & Dziewonski, A. M. (1985). Lower mantle heterogeneity, dynamic topography, and the geoid. *Nature*, *313*(6003), 541–545. https://doi.org/10.1038/313541a0

Hanan, B. B., & Graham, D. W. (1996). Lead and helium isotope evidence from oceanic basalts for a common deep source of mantle plumes. *Science*, *272*(5264), 991–995. https://doi.org/10.1126/science.272.5264.991

Hanan, B. B., & Schilling, J.-G. (1997). The dynamic evolution of the Iceland mantle plume: The lead isotope perspective. *Earth and Planetary Science Letters*, *151*(1-2), 43–60. https://doi.org/10.1016/S0012-821X(97)00105-2

Hart, S. R. (1984). A large-scale isotope anomaly in the Southern Hemisphere mantle. *Nature*, *309*(5971), 753–757. https://doi.org/10.1038/309753a0

Hart, S. R. (1988). Heterogeneous mantle domains: Signatures, genesis and mixing chronologies. *Earth and Planetary Science Letters*, *90*, 273–296.

Hart, S. R., Hauri, E. H., Oschmann, L. A., & Whitehead, J. A. (1992). Mantle plumes and entrainment: Isotopic evidence. *Science*, *256*(5056), 517–520. https://doi.org/10.1126/science.256.5056.517

Harvey, J., Gannoun, A., Burton, K. W., Rogers, N. W., Alard, O., & Parkinson, I. J. (2006). Ancient melt extraction from the oceanic upper mantle revealed by Re–Os isotopes in abyssal peridotites from the Mid-Atlantic ridge. *Earth and Planetary Science Letters*, *244*, 606–621.

He, Y., & Wen, L. (2012). Geographic boundary of the "Pacific Anomaly" and its geometry and transitional structure in the north. *Journal of Geophysical Research*, *117*, B09308. https://doi.org/10.1029/2012JB009436

Hernlund, J. W., & McNamara, A. K. (2015). Dynamics of the core-mantle boundary region. In *Treatise on Geophysics* (2nd ed., Vol. 7, pp. 461–519). Amsterdam: Elsevier.

Hirose, K., Fei, Y. W., Ma, Y. Z., & Mao, H. K. (1999). The fate of subducted basaltic crust in the Earth's lower mantle. *Nature*, *397*(6714), 53–56. https://doi.org/10.1038/16225

Hofmann, A. W. (1997). Mantle geochemistry: The message from oceanic volcanism. *Nature*, *385*(6613), 219–229. https://doi.org/10.1038/385219a0

Hofmann, A. W., & White, W. M. (1982). Mantle plumes from ancient oceanic crust. *Earth and Planetary Science Letters*, *57*, 421–436.

Homrighausen, S., Hoernle, K., Hauff, F., Geldmacher, J., Wartho, J.-A., Van den Bogaard, P., & Garbe-Schönberg, D. (2018). Global distribution of the HIMU end member: Formation through Archean plume-lid tectonics. *Earth-Science Reviews*, *182*, 85–101. https://doi.org/10.1016/j.earscirev.2018.04.009

Ito, G., & Mahoney, J. (2005a). Flow and melting of a heterogeneous mantle. 1: Importance to the geochemistry of ocean island and mid-ocean ridge basalts. *Earth and Planetary Science Letters*, *230*, 29–46.

Ito, G., & Mahoney, J. J. (2005b). Flow and melting of a heterogeneous mantle: 2. Implications for a chemically nonlayered mantle. *Earth and Planetary Science Letters*, *230*(1-2), 47–63. https://doi.org/10.1016/j.epsl.2004.10.034

Ito, G., & Mahoney, J. J. (2006). Melting a high ^{3}He/^{4}He source in a heterogeneous mantle. *Geochemistry, Geophysics, Geosystems*, *7*, Q05010. https://doi.org/10.1029/2005GC001158

Jackson, M. G., Becker, T. W., & Konter, J. G. (2018). Evidence for a deep mantle source for EM and HIMU domains from integrated geochemical and geophysical constraints. *Earth and Planetary, Science Letters*, *484*, 1–14.

Jackson, M. G., Konter, J. G., & Becker, T. W. (2017). Primordial helium entrained by the hottest mantle plumes. *Nature*, *542*(7641), 340–343. https://doi.org/10.1038/nature21023

Jellinek, A. M., & Manga, M. (2004). Links between long-lived hot spots, mantle plumes, D, and plate tectonics. *Reviews of Geophysics*, *42*, RG3002. https://doi.org/10.1029/2003RG000144

King, S. D., & Adam, C. (2014). Hotspot swells revisited. *Physics of the Earth and Planetary Interiors*, *235*, 66–83. https://doi.org/10.1016/j.pepi.2014.07.006

Knittle, E., & Jeanloz, R. (1989). Simulating the core–mantle boundary: An experimental study of high-pressure reactions between silicates and liquid iron. *Geophysical Research Letters*, *16*, 609–612. https://doi.org/10.1029/GL016i007p00609

Kokfelt, T. F., Hoernle, K., Hauff, F., Fiebig, J., Werner, R., & Garbe-Schönberg, D. (2006). Combined trace element and Pb-Nd-Sr-O isotope evidence for recycled oceanic crust (upper and lower) in the Iceland mantle plume. *Journal of Petrology*, *47*, 1705–1749.

Konrad, K., Koppers, A. A. P., Steinberger, B., Finlayson, V. A., Konter, J. G., & Jackson, M. G. (2018). On the relative motions of long-lived Pacific mantle plumes. *Nature Communications*, *9*(1), 854. https://doi.org/10.1038/s41467-018-03277-x

Konter, J. G., & Becker, T. W. (2012). Shallow lithospheric contribution to mantle plumes revealed by integrating seismic and geochemical data. *Geochemistry, Geophysics, Geosystems*, *13*, Q02004. https://doi.org/10.1029/2011GC003923

Konter, J. G., Hanan, B. B., Blichert-Toft, J., Koppers, A. A. P., Plank, T., & Staudigel, H. (2008). One hundred million years of mantle geochemical history suggest the retiring of mantle plumes is premature. *Earth and Planetary Science Letters*, *275*(3-4), 285–295. https://doi.org/10.1016/j.epsl.2008.08.023

Kumagai, I., Davaille, A., Kurita, K., & Stutzmann, E. (2008). Mantle plumes: Thin, fat, successful, or failing? Constraints to explain hot spot volcanism through time and space. *Geophysical Research Letters*, *35*, L16301. https://doi.org/10.1029/2008GL035079

Labrosse, S., Hernlund, J. W., & Coltice, N. A. (2007). A crystallizing dense magma ocean at the base of the Earth's mantle. *Nature*, *450*(7171), 866–869. https://doi.org/10.1038/nature06355

Lee, C. T. A., Luffi, P., Höink, T., Li, J., Dasgupta, R., & Hernlund, J. (2010). Upside-down differentiation and generation of a 'primordial' lower mantle. *Nature*, *463*(7283), 930–933. https://doi.org/10.1038/nature08824

Lekic, V., Cottaar, S., Dziewonski, A., & Romanowicz, B. (2012). Cluster analysis of global lower mantle tomography: A new class of structure and implications for chemical heterogeneity. *Earth and Planetary Science Letters*, *357–358*, 68–77.

Li, M., McNamara, A. K., & Garnero, E. J. (2014). Chemical complexity of hotspots caused by cycling oceanic crust through mantle reservoirs. *Nature Geoscience*, *7*(5), 366–370. https://doi.org/10.1038/ngeo2120

Liu, C.-Z., Snow, J. E., Hellebrand, E., Brügmann, G., von der Handt, A., Büchl, A., & Hofmann, A. W. (2008). Ancient, highly heterogeneous mantle beneath Gakkel ridge, Arctic Ocean. *Nature*, *452*(7185), 311–316. https://doi.org/10.1038/nature06688

Maclennan, J. (2008). Concurrent mixing and cooling of melts under Iceland. *Journal of Petroleum*, *49*(11), 1931–1953. https://doi.org/10.1093/petrology/egn052

Maclennan, J., McKenzie, D., Grönvold, K., Shimizu, N., Eiler, J. M., & Kitchen, N. (2003). Melt mixing and crystallization under Theistareykir, northeast Iceland. *Geochemistry, Geophysics, Geosystems*, 4, 8624. https://doi.org/10.1029/2003GC000558

Macpherson, C. G., Hilton, D. R., Sinton, J. M., Poreda, R. J., & Craig, H. (1998). High ^{3}He/^{4}He ratios in Manus backarc basin: Implications for mantle mixing and the origin of plume in the western Pacific Ocean. *Geology*, *26*(11), 1007–1010. https://doi.org/10.1130/0091-7613(1998)026<1007:HHHRIT>2.3.CO;2

Masters, G., Laske, G., Bolton, H., & Dziewonski, A. (2000). The relative behavior of shear velocity, bulk sound speed, and compressional velocity in the mantle: Implications for chemical and thermal structure. In S. Karato (Ed.), *Earth's deep interior: Mineral physics and tomography*, *AGU Monograph* (Vol. 117, pp. 63–87). Washington, DC: American Geophysical Union.

McNamara, A. K., Garnero, E. J., & Rost, S. (2010). Tracking deep mantle reservoirs with ultra low velocity zones. *Earth and Planetary Science Letters*, *299*, 1–9.

McNamara, A. K., & Zhong, S. (2004). Thermochemical structures within a spherical mantle: Superplumes or piles? *Journal of Geophysical Research*, *109*, B07402. https://doi.org/10.1029/2003JB002847

McNamara, A. K., & Zhong, S. (2005). Thermochemical structures beneath Africa and the Pacific Ocean. *Nature*, *347*, 1136–1139.

Montelli, R., Nolet, G., Dahlen, F. A., & Masters, G. (2006). A catalogue of deep mantle plumes: New results from finite-frequency tomography. *Geochemistry, Geophysics, Geosystems*, *7*, Q11007. https://doi.org/10.1029/2006GC001248

Mukhopadhyay, S. (2012). Early differentiation and volatile accretion recorded in deep-mantle neon and xenon. *Nature*, *486*(7401), 101–104. https://doi.org/10.1038/nature11141

Mulyukova, E., Steinberger, B., Dabrowski, M., & Sobolev, S. V. (2015). Survival of LLSVPs for billions of years in a vigorously convecting mantle: Replenishment and destruction of chemical anomaly. *Journal of Geophysical Research: Solid Earth*, *120*, 3824–3847. https://doi.org/10.1002/2014JB011688

Mundl, A., Touboul, M., Jackson, M. G., Day, J. M. D., Kurz, M. D., Lekic, V., et al. (2017). Tungsten-182 heterogeneity in modern ocean island basalts. *Science*, *356*(6333), 66–69. https://doi.org/10.1126/science.aal4179

Nakagawa, T., & Tackley, P. J. (2014). Influence of combined primordial layering and recycled MORB on the coupled thermal evolution of Earth's mantle and core. *Geochemistry, Geophysics, Geosystems*, *15*, 619–633. https://doi.org/10.1002/2013GC005128

Nakagawa, T., Tackley, P. J., Deschamps, F., & Connolly, J. A. (2010). The influence of MORB and harzburgite composition on thermo-chemical mantle convection in a 3-D spherical shell with self-consistently calculated mineral physics. *Earth and Planetary Science Letters*, *296*, 403–412.

Qin, Y., Capdeville, Y., Montagner, J.-P., Boschi, L., Becker, T. W., & T. W. (2009). Reliability of mantle tomography models assessed by spectral-element simulation. *Geophysical Journal International*, *177*(1), 125–144. https://doi.org/10.1111/j.1365-246X.2008.04032.x

Ritsema, J., Deuss, A., van Heijst, J. J., & Woodhouse, J. H. (2011). S40RTS: A degree-40 shear-velocity model for the mantle from new Rayleigh wave dispersion, teleseismic traveltime and normal-mode splitting function measurements. *Geophysical Journal International*, *184*(3), 1223–1236. https://doi.org/10.1111/j.1365-246X.2010.04884.x

Rost, S., Earle, P. S., Shearer, P., Frost, D. A., & Selby, N. D. (2015). In A. Khan & F. Deschamps (Eds.), *The Earth's heterogeneous mantle: A Geophysical, geodynamical, and geochemical perspective* (pp. 367–390). Cham, Heidelberg, New York, Dordrecht, and London: Springer Publishing. https://doi.org/10.1007/978-3-319-15627-9

Rudge, J. F., Maclennan, J., & Stracke, A. (2013). The geochemical consequences of mixing melts from a heterogeneous mantle. *Geochimica et Cosmochimica Acta*, *114*, 112–143. https://doi.org/10.1016/j.gca.2013.03.042

Shorttle, O., Maclennan, J., & Lambart, S. (2014). Quantifying lithological variability in the mantle. *Earth and Planetary Science Letters*, *395*, 24–40.

Shorttle, S., Rudge, J., Maclennan, J., & Rubin, K. (2016). A statistical description of concurrent mixing and crystallisation during MORB differentiation: Implications for trace element enrichment. *Journal of Petroleum*, *57*, 1–33.

Simmons, N. A., Forte, A. M., Boschi, L., & Grand, S. P. (2010). GyPSuM: A joint tomographic model of mantle density and seismic wave speeds. *Journal of Geophysical Research*, *115*, B12310. https://doi.org/10.1029/2010JB007631

Steinberger, B., & Antretter, M. (2006). Conduit diameter and buoyant rising speed of mantle plumes: Implications for the motion of hot spots and shape of plume conduits. *Geochemistry, Geophysics, Geosystems*, *7*, Q11018. https://doi.org/10.1029/2006GC001409

Stracke, A. (2012). Earth's heterogeneous mantle: A product of convection-driven interaction between crust and mantle. *Chemical Geology*, *330–331*, 274–299.

Stracke, A., & Bourdon, B. (2009). The importance of melt extraction for tracing mantle heterogeneity. *Geochimica et Cosmochimica Acta*, *73*(1), 218–238. https://doi.org/10.1016/j.gca.2008.10.015

Stracke, A., Hofmann, A. W., & Hart, S. R. (2005). FOZO, HIMU, and the rest of the mantle zoo. *Geochemistry, Geophysics, Geosystems*, *6*, Q05007. https://doi.org/10.1029/2004GC000824

Tackley, P. J. (1998). Three-dimensional simulations of mantle convection with a thermochemical CMB boundary layer: D″? In Gurnis, et al. (Eds.), *The Core–Mantle Boundary Region* (pp. 231–253). Washington, DC: American Geophysical Union.

Tackley, P. J. (2000). Mantle convection and plate tectonics: Toward an integrated physical and chemical theory. *Science*, *288*(5473), 2002–2007. https://doi.org/10.1126/science.288.5473.2002

Tackley, P. J. (2002). Strong heterogeneity caused by deep mantle layering. *Geochemistry, Geophysics, Geosystems*, *3*(4), 1024. https://doi.org/10.1029/2001GC000167

Thorne, M. S., Garnero, E. J., & Grand, S. P. (2004). Geographic correlation between hot spots and deep mantle lateral shear-wave velocity gradients. *Physics of the Earth and Planetary Interiors*, *146*(1-2), 47–63. https://doi.org/10.1016/j.pepi.2003.09.026

Tolstikhin, I. N., Kramers, J. D., & Hofmann, A. W. (2006). A chemical earth model with whole mantle convection: The importance of a core–mantle boundary layer (D″) and its early formation. *Chemical Geology*, *226*(3-4), 79–99. https://doi.org/10.1016/j.chemgeo.2005.09.015

Torsvik, T. H., Smethurst, M. A., Burke, K., & Steinberger, B. (2006). Large igneous provinces generated from the margins of the largelow-velocity provinces in the deep mantle. *Geophysical Journal International*, *167*(3), 1447–1460. https://doi.org/10.1111/j.1365-246X.2006.03158.x

Warren, J. M. (2016). Global variations in abyssal peridotite compositions. *Lithos*, *248*, 193–219.

Warren, J. M., & Shirey, S. B. (2012). Lead and osmium isotopic constraints on the oceanic mantle from single abyssal peridotite sulfides. *Earth and Planetary Science Letters*, *359*, 279–293.

Weis, D., Garcia, M. O., Rhodes, J. M., Jellinek, M., & Scoates, J. S. (2011). Role of the deep mantle in generating the compositional asymmetry of the Hawaiian mantle plume. *Nature Geoscience*, *4*, 831–838.

White, W. M. (2015). Isotopes, DUPAL, LLSVPs, and Anekantavada. *Chemical Geology*, *419*, 10–28. https://doi.org/10.1016/j.chemgeo.2015.09.026

White, W. M., & Hofmann, A. W. (1982). Sr and Nd isotope geochemistry of oceanic basalts and mantle evolution. *Nature*, *296*(5860), 821–825. https://doi.org/10.1038/296821a0

Williams, C. D., Li, M., McNamara, A. K., Garnero, E. J., & van Soest, M. C. (2015). Episodic entrainment of deep primordial mantle material into ocean island basalts. *Nature Communications*, *6*(1), 8937. https://doi.org/10.1038/ncomms9937

Williams, Q., Revenaugh, J., & Garnero, E. (1998). A correlation between ultra-low basal velocities in the mantle and hot spots. *Science*, *281*(5376), 546–549. https://doi.org/10.1126/science.281.5376.546

Yu, S., & Garnero, E. J. (2018). Ultra-low velocity zone locations: A global assessment. *Geochemistry, Geophysics, Geosystems*, *19*, 396–414. https://doi.org/10.1002/2017GC007281

Zhang, N., Zhong, S., Leng, W., & Li, Z.-X. (2010). A model for the evolution of the Earth's mantle structure since the Early Paleozoic. *Journal of Geophysical Research*, *115*, B06401. https://doi.org/10.1029/2009JB006896

Zhong, S., Zhang, N., Li, Z.-X., & Roberts, J. H. (2007). Supercontinent cycles, true polar wander, and very long-wavelength mantle convection. *Earth and Planetary Science Letters*, *261*, 551–564.

Zindler, A., & Hart, S. (1986). Chemical geodynamics. *Annual Review of Earth and Planetary Sciences*, *14*(1), 493–571. https://doi.org/10.1146/annurev.ea.14.050186.002425